Article

Neuron

Cytoplasmic TDP-43 De-mixing Independent of Stress Granules Drives Inhibition of Nuclear Import, Loss of Nuclear TDP-43, and Cell Death

Graphical Abstract

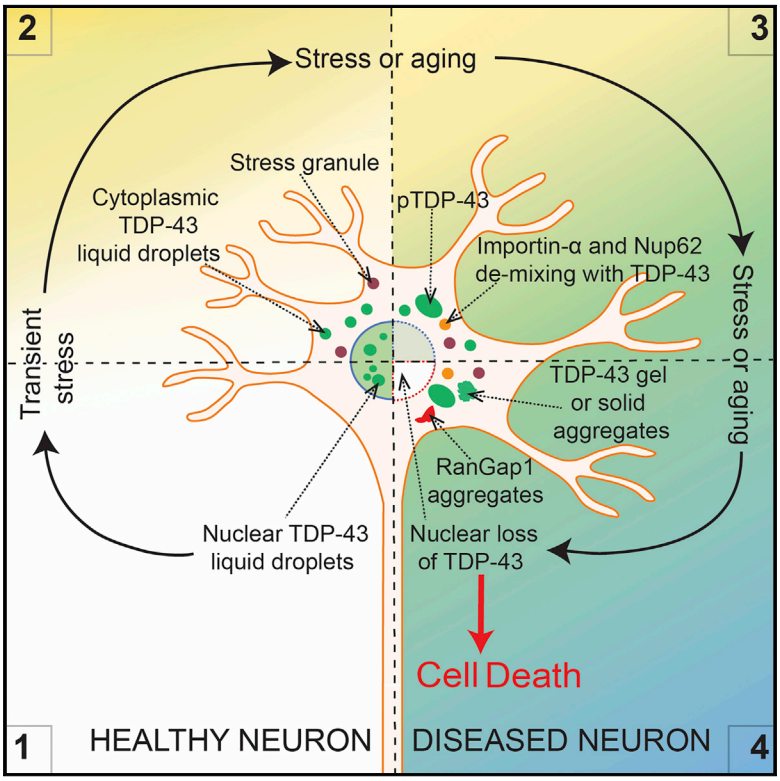

Highlights

- Transient stress induces long-lasting phase separation of cytoplasmic TDP-43
- Formation/maintenance of phase separated TDP-43 is independent of stress granules
- Phase-separated TDP-43 inhibits nuclear transport by de-mixing importin-α and Nup62
- Cytoplasmic TDP-43 de-mixing depletes nuclear TDP-43 and induces cell death

Authors

Fatima Gasset-Rosa, Shan Lu, Haiyang Yu, ..., James Shorter, Sandrine Da Cruz, Don W. Cleveland

Correspondence

sdacruz@ucsd.edu (S.D.C.), dcleveland@ucsd.edu (D.W.C.)

In Brief

TDP-43 aggregation is the major hallmark of multiple neurodegenerative diseases, including ALS and FTD. Gasset-Rosa et al. demonstrate that transient stress induces long-lasting cytoplasmic TDP-43 de-mixing independent of stress granules, driving nuclear import defects, nuclear TDP-43 clearance, and cell death.

Gasset-Rosa et al., 2019, Neuron *102*, 339–357
April 17, 2019
https://doi.org/10.1016/j.neuron.2019.02.038

CellPress

Neuron
Article

Cytoplasmic TDP-43 De-mixing Independent of Stress Granules Drives Inhibition of Nuclear Import, Loss of Nuclear TDP-43, and Cell Death

Fatima Gasset-Rosa,[1,4] Shan Lu,[1,4] Haiyang Yu,[1,4] Cong Chen,[1,4] Ze'ev Melamed,[1] Lin Guo,[3] James Shorter,[3] Sandrine Da Cruz,[1,*] and Don W. Cleveland[1,2,5,*]
[1]Ludwig Institute for Cancer Research, University of California at San Diego, La Jolla, CA 92093, USA
[2]Department of Cellular and Molecular Medicine, University of California at San Diego, La Jolla, CA 92093, USA
[3]Department of Biochemistry & Biophysics, University of Pennsylvania, Philadelphia, PA 19104-6059, USA
[4]These authors contributed equally
[5]Lead Contact
*Correspondence: sdacruz@ucsd.edu (S.D.C.), dcleveland@ucsd.edu (D.W.C.)
https://doi.org/10.1016/j.neuron.2019.02.038

SUMMARY

While cytoplasmic aggregation of TDP-43 is a pathological hallmark of amyotrophic lateral sclerosis and frontotemporal dementia, how aggregates form and what drives its nuclear clearance have not been determined. Here we show that TDP-43 at its endogenous level undergoes liquid-liquid phase separation (LLPS) within nuclei in multiple cell types. Increased concentration of TDP-43 in the cytoplasm or transient exposure to sonicated amyloid-like fibrils is shown to provoke long-lived liquid droplets of cytosolic TDP-43 whose assembly and maintenance are independent of conventional stress granules. Cytosolic liquid droplets of TDP-43 accumulate phosphorylated TDP-43 and rapidly convert into gels/solids in response to transient, arsenite-mediated stress. Cytoplasmic TDP-43 droplets slowly recruit importin-α and Nup62 and induce mislocalization of RanGap1, Ran, and Nup107, thereby provoking inhibition of nucleocytoplasmic transport, clearance of nuclear TDP-43, and cell death. These findings identify a neuronal cell death mechanism that can be initiated by transient-stress-induced cytosolic de-mixing of TDP-43.

INTRODUCTION

Mislocalization, self-assembly, and aggregation of misfolded TAR DNA-binding protein 43 (TDP-43) in the cytoplasm of affected motor neurons is a common neuropathological hallmark of almost all cases of amyotrophic lateral sclerosis (ALS) (Neumann et al., 2006). Proteinaceous inclusions, containing misfolded aggregated proteins or fragments of them, are also found in each of the major neurodegenerative disorders, including Alzheimer's (AD), Parkinson's (PD), frontotemporal dementia (FTD), and Huntington's (HD) diseases (Chiti and Dobson, 2006). Many of the aggregated proteins contain intrinsically disordered protein domains that are enriched in, or composed of, only a few amino acids and are referred to as low complexity (LC) domains. These domains display a sequence-intrinsic conformational heterogeneity (i.e., disorder) characteristic of intrinsically disordered proteins and/or regions (Boeynaems et al., 2018). LC domains are also present in yeast prion proteins, which have the ability to interconvert into amyloid fibers (King et al., 2012). Prion-like LC domains are particularly abundant in RNA- and DNA-binding proteins, and their amino acid composition has been conserved across evolution (King et al., 2012; Malinovska et al., 2013).

TDP-43 is an RNA-binding protein that localizes predominantly in the nucleus and is thought to shuttle between the cytoplasm and nucleus (Ayala et al., 2008). It forms abnormal cytoplasmic aggregates (Neumann et al., 2006) in neurons and glia in more than 90% of ALS and 45% of FTD cases. These two progressive neurodegenerative diseases, which share genetic and pathological features (Ling et al., 2013), are without effective treatments to slow fatal disease progression (Taylor et al., 2016). Discovery of missense mutations in TDP-43 in patients with ALS or FTD (Rutherford et al., 2008; Sreedharan et al., 2008) demonstrated a direct link between genetic variants and TDP-43 pathology. Many mechanisms have been proposed to explain the abnormal cytosolic accumulation of TDP-43 and the progressive spreading of TDP-43 pathology.

TDP-43 contains a prion-like, LC domain that is glycine, glutamine, and asparagine rich and is predominantly an intrinsically disordered region (IDR) (Conicella et al., 2016), which renders TDP-43 intrinsically aggregation prone (Johnson et al., 2009). Disordered domains of RNA-binding proteins can drive dynamic self-assembly into intracellular membraneless organelles, including P granules (paranuclear granules in germline cells of *C. elegans*), nucleoli, and stress granules, each of which has been reported to fuse, minimize surface tension, and dynamically exchange components with the solution, all properties indicative of liquid-like behavior (Brangwynne et al., 2009; Mitrea and Kriwacki, 2016). Correspondingly, phase separation might be the operational principle governing the formation of membraneless organelles. A key unresolved issue is whether (and, if so, how) assembly into membraneless organelles

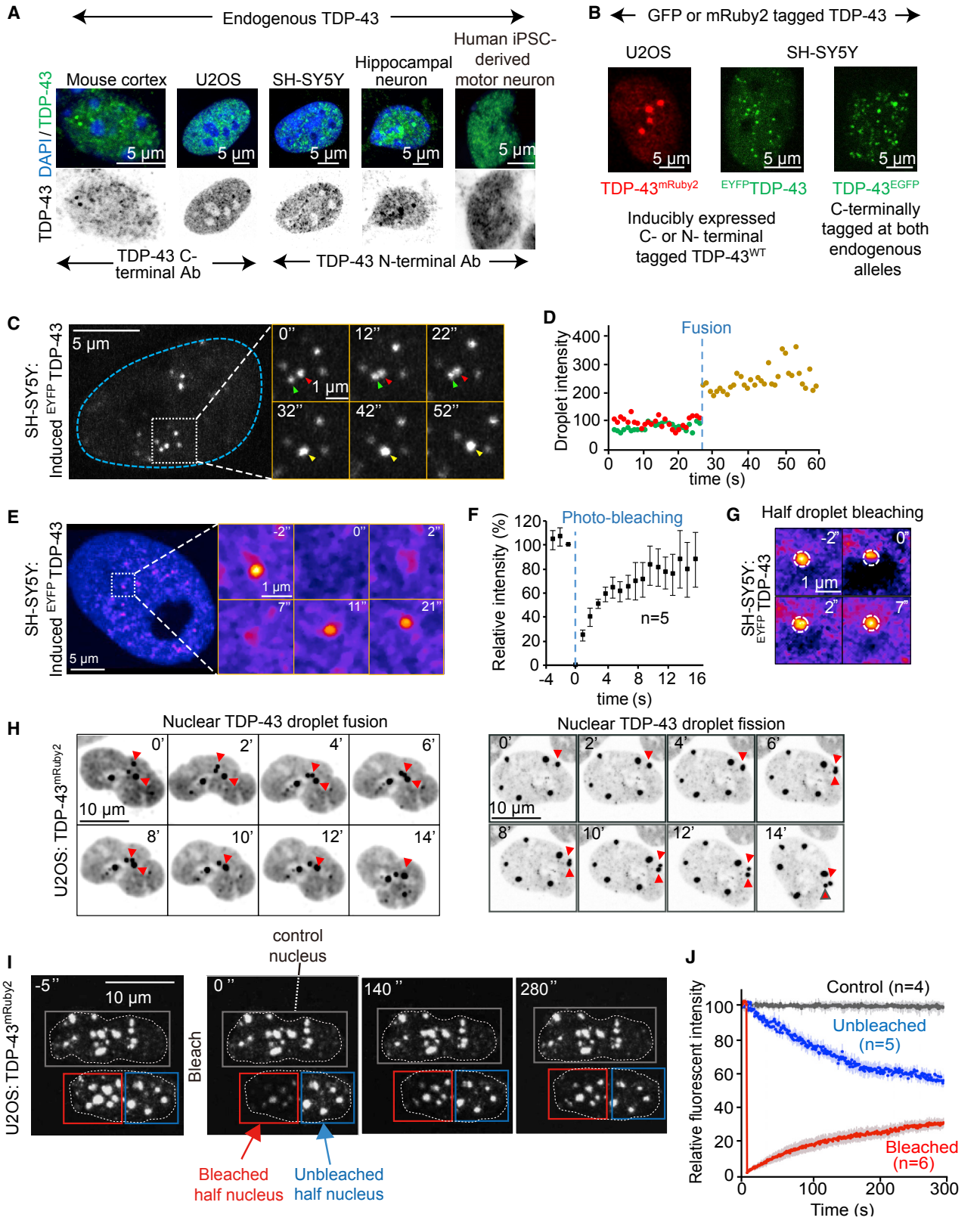

(legend on next page)

regulates or affects biological function(s) of their constituent proteins. Beyond that, phase-separated droplets have increasingly been implicated as crucibles for nucleation of pathologic protein aggregation since protein concentration is expected to be sharply increased within the droplets (Li et al., 2013; Ramaswami et al., 2013).

Prion-like LC-domain-containing heterogeneous nuclear ribonucleoproteins (hnRNPs), such as FUS, hnRNPA1, and TIA1 (other proteins whose mutation is causative of ALS/FTD), exhibit liquid-liquid phase separation (LLPS) as purified proteins *in vitro* (Burke et al., 2015; Mackenzie et al., 2017; Mateju et al., 2017; Molliex et al., 2015; Patel et al., 2015). TDP-43 has been reported to display aspects (round-shaped morphology or fusion events) of liquid-phase separation *in vitro* (Conicella et al., 2016; Ryan et al., 2018; Wang et al., 2018). Prolonged LLPS of purified FUS or repeated cycles of temperature-dependent de-mixing of mutant hnRNPA1 can induce conversion to a solid phase (Molliex et al., 2015; Patel et al., 2015), while expression of FUS variants with decreased ability to bind RNA can form solid-like aggregates in a cancer cell line (Maharana et al., 2018). The relevance of this altered phase behavior is not established in disease; however, as in every reported instance, the presence of other proteins or post-translationally modified variants inhibits liquid-phase separation *in vitro* (Guo et al., 2018; Hofweber et al., 2018; Qamar et al., 2018; Yoshizawa et al., 2018). Only a handful of observations confirm LLPS properties of these RNPs in living cells, and in most examples, de-mixing requires extreme conditions, including transient overexpression or degradation of total cellular RNA or both (Gopal et al., 2017; Maharana et al., 2018; Wang et al., 2018).

No effort has succeeded in identifying whether TDP-43 undergoes liquid-liquid de-mixing in the cytoplasm—where pathological aggregates accumulate—and, if so, whether such de-mixing can trigger nuclear loss of TDP-43, conversion of TDP-43 to an aggregated state, or both. Here we identify intranuclear LLPS of native TDP-43 in multiple mammalian cells in cultured mouse cortical neurons and human iPSC-derived motor neurons. Arsenite-mediated stress is shown to induce TDP-43 de-mixing into cytoplasmic liquid droplets that are independent of stress granule components or formation and that rapidly convert to gels/solids that recruit phosphorylated TDP-43. Transient stress from exposure to fragmented amyloid-like fibrils induces endogenous TDP-43 de-mixing into cytosolic droplets that (1) form and persist for up to 1 month, (2) are independent of conventional stress granules, (3) accumulate phosphorylated TDP-43, (4) compromise nucleo-cytoplasmic transport, (5) slowly deplete nuclear TDP-43, and (6) ultimately elicit cell death.

RESULTS

Nuclear TDP-43 De-mixes under Physiological Conditions

While use of immunofluorescence has established that TDP-43 is primarily intranuclear, high-resolution inspection (using N- or C-terminal antibodies) of endogenous TDP-43 revealed that it is not distributed diffusely in nucleoplasm but rather forms rounded particles in both mouse and human cells, including cortical neurons from wild-type mouse brain, primary cultured mouse hippocampal neurons, human SH-SY5Y neuronal-like cells, U2OS, a human non-neuronal cell line, and motor neurons induced from human pluripotent stem cells (iPSCs) (Figure 1A). An apparently de-mixed distribution was confirmed by imaging directly fluorescently tagged TDP-43 expressed at levels equal to or below the normal endogenous level (Figure S1). Accumulation of (1) an amino-terminally EYFP-tagged TDP-43 (^{EYFP}TDP-43) to about one-third the level of endogenous TDP-43 (Figures S1A and S1B) or (2) a carboxy-terminally mRuby2-tagged TDP-43 (TDP-43^{mRuby2}) replacing endogenous TDP-43 (Figure S1C) yielded between 5 and 50 rounded, droplet-like particles of 0.2–1 μm diameter in each nucleus (Figure 1B). Similar rounded particles were found (Figure 1B) in SH-SY5Y cells that had been genome edited at both TDP-43 alleles to encode fluorescently tagged TDP-43 (TDP-43^{EGFP}), a variant that confers the essential functions of TDP-43 (Figures S1D and S1E).

Live cell imaging was used to determine that these intranuclear TDP-43 particles have liquid-like properties. Fusion events

Figure 1. Nuclear TDP-43 De-mixes under Physiological Conditions

(A) Endogenous TDP-43 detected by immunofluorescence (green) in multiple cell types (upper panels). Endogenous TDP-43 (green) and DAPI (blue); (lower panels) TDP-43 only (inverted in gray).

(B) Representative images of nuclear particles of full-length TDP-43 in U2OS or SH-SY5Y cells stably or inducibly expressing wild-type TDP-43 C-terminally tagged with mRuby2 (TDP-43^{mRuby2}; left) or N-terminally tagged with EYFP (^{EYFP}TDP-43; middle), respectively. C-terminally EGFP-tagged TDP-43 expressed from both endogenous alleles in SH-SY5Y (right panel).

(C) Representative fusion event of nuclear ^{EYFP}TDP-43 droplets in SH-SY5Y cells 24 h post induction of ^{EYFP}TDP-43 expression. Higher magnification is shown in the right panels. The green and red arrowheads point to two separated droplets before fusion, while the yellow one points to the fused droplet.

(D) Fluorescence intensity of the indicated droplets in (C) before (red and green arrowheads) and after (yellow arrowhead) fusion, normalized to average droplet intensity before fusion.

(E) FRAP of ^{EYFP}TDP-43 droplets in SH-SY5Y cells after 24 h of expression. Higher magnification is shown in the right panel. The whole droplet was photobleached at 0″.

(F) Mean fluorescence intensity at the bleached area shown in (E) plotted over time, normalized to the average intensity of a droplet before photobleaching and represented as mean ± SEM (from the recovery curves of five droplets in a total of three independent experiments).

(G) FRAP of partial photobleaching of ^{EYFP}TDP-43 droplets in SH-SY5Y cells 24 h after ^{EYFP}TDP-43 induction.

(H) Fusion and fission events of TDP-43^{mRuby2} droplets in U2OS cells. Red arrowheads point to fusing or dividing droplets.

(I) FRAP of nuclear TDP-43^{mRuby2} in U2OS cells. Half of one nucleus (outlined by the red box) was photobleached at 0″. The blue box outlines the unbleached area of the other half of the nucleus; the gray box outlines an unbleached control nucleus in an adjacent cell.

(J) Mean fluorescence intensity (normalized to the unbleached control nucleus) in the bleached and unbleached areas shown in (I) plotted over time (represented as mean ± SEM from the recovery curves of three nuclei in a total of three independent experiments).

See also Figure S1.

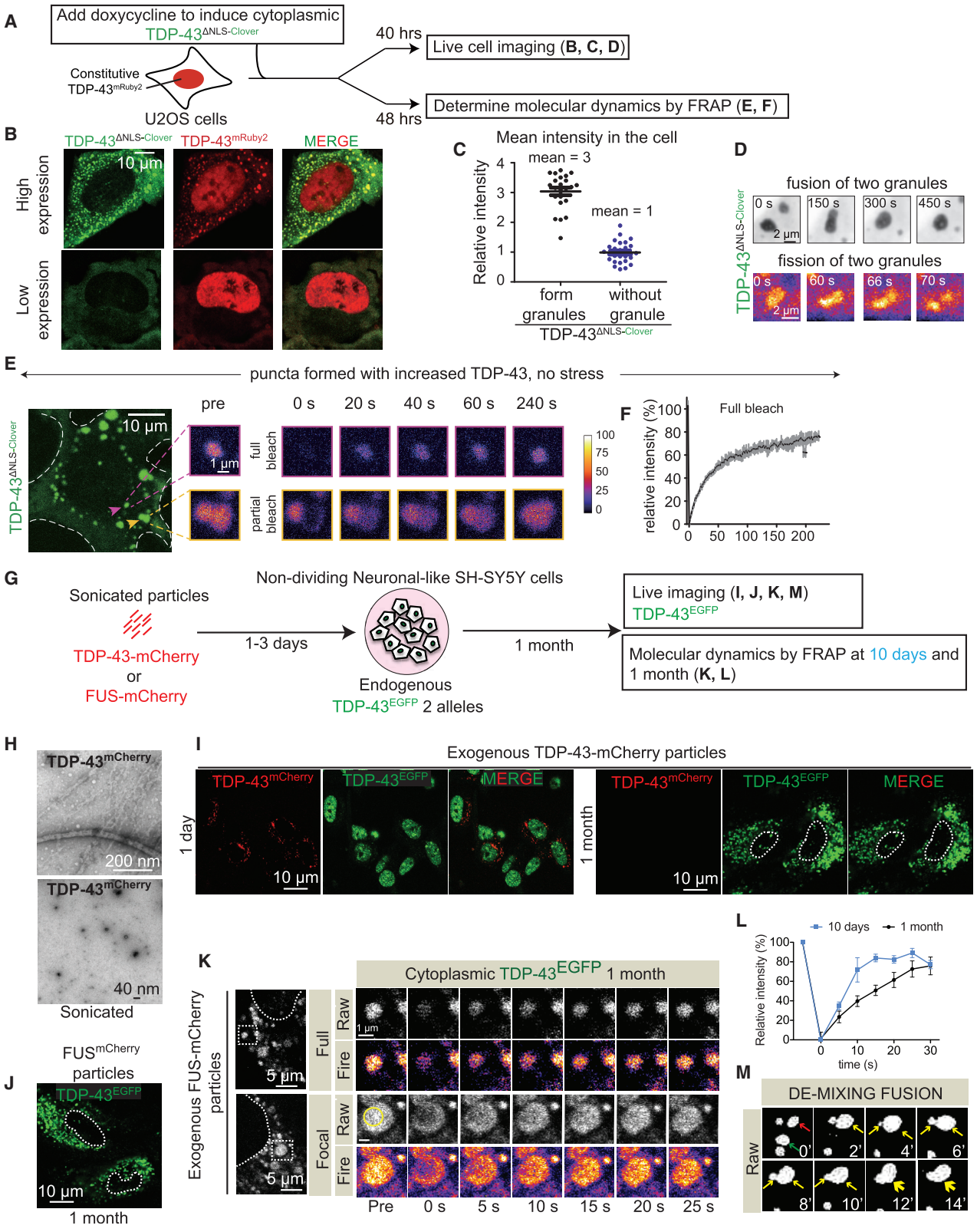

(legend on next page)

could be observed frequently within a 10 s period of monitoring in neuron-like SH-SY5Y cells (see, for example, the fusion of two ^{EYFP}TDP-43 droplets labeled with green or red arrowheads in Figures 1C and 1D). Fluorescence recovery after photobleaching of whole ^{EYFP}TDP-43-containing droplets in SH-SY5Y revealed rapid recovery (to ~70% of original intensity) in <10 s (Figures 1E and 1F), indicating fast molecular exchange of TDP-43 molecules between droplets and nucleoplasm. Internal molecular dynamics were five times faster, with fluorescence intensity re-equilibrated within 2 s following half-droplet bleaching (Figure 1G). Fusion events were also documented for TDP-43^{mRuby2}- and TDP43^{EGFP}-containing droplets in U2OS or SH-SY5Y cells (Figures 1H and S1F, respectively). Fission events were also observed (Figure 1H, right panel), albeit at much lower frequency. As expected for LLPS, after photobleaching half of a nucleus, fluorescence intensity of TDP-43 recovered in the bleached half within 140 s, with a corresponding decrease in intensity in the unbleached half (Figures 1I and 1J). Thus, TDP-43 phase separates in normal physiological conditions into intranuclear liquid droplets in which TDP-43 molecules dynamically move into and out of the droplets.

Concentration-Dependent TDP-43 De-Mixing in the Cytoplasm

To mimic the increased accumulation of cytoplasmic TDP-43 during aging expected from the known age-dependent loss of nuclear pore components (D'Angelo et al., 2009), we expressed fluorescently tagged TDP-43 with a disrupted NLS (TDP-43$^{\Delta NLS\text{-}Clover}$) using a doxycycline-inducible system in human U2OS cells that also stably express TDP-43^{mRuby2} (Figure 2A) at the endogenous TDP-43 level (Figure S1C). Induction of TDP-43$^{\Delta NLS\text{-}Clover}$ produced a range of accumulation of cytoplasmic TDP-43 in individual cells, with Clover (and mRuby2) fluorescence providing a direct readout of TDP-43 level (Figures 2B and 2C). Increased accumulation of cytoplasmic TDP-43 was sufficient to induce its de-mixing into 1–3 μm spherical, cytoplasmic particles (Figure 2B) that (1) over time recruited the initially nuclear TDP-43^{mRuby2} (Figure 2B) and (2) underwent fusions and fissions (Figure 2D). TDP-43 cytoplasmic droplets remained liquid over extended periods, with rapid and efficient (70%) recovery (within 2 or 4 min, respectively) after complete or partial photobleaching (Figures 2E and 2F). Thus, an increased level of cytoplasmic TDP-43 is sufficient to induce its de-mixing in the cytoplasm.

TDP-43 Cytoplasmic De-Mixing into Liquid Droplets

To determine whether nuclear TDP-43 could redistribute to the cytoplasm and de-mix, we genetically edited both TDP-43 alleles in SH-SY5Y cells to express physiological levels of wild-type TDP-43 fused to a green fluorescent protein (TDP-43^{EGFP}) (Figures S1D and S1E). Non-dividing neuronal-like (SH-SY5Y) cells were then transiently exposed to fragmented amyloid-like-containing fibrils. mCherry-tagged recombinant TDP-43 (or FUS) was purified (Figure S2A) and incubated for 24 h at 20°C. Both were self-assembled into fibrils whose appearance (Figures 2H and S2B) was highly similar to amyloid-like fibrils (Rambaran and Serpell, 2008). After sonication, the fragmented fibrils (~20 nm in size) were added to the culture media of SH-SY5Y cells expressing TDP-43^{EGFP} from both endogenous TDP-43 alleles (Figures 2G and 2H and S2B). As expected, without fibril addition, TDP-43^{EGFP} remained nuclear without cytoplasmic liquid-like structures in non-cycling cells arrested in the G1 cell-cycle phase (Figure S2C).

After transient addition of TDP-43^{mCherry} sonicated fibrils (Figures 2G and 2H), time-lapse confocal imaging was used to (1) determine that fibril fragments were internalized within 12 h, (2) follow the fate of the fibrils, and (3) determine localization of TDP-43^{EGFP} expressed at endogenous levels. At early times, fragmented TDP-43 fibrils accumulated in the cytoplasm but did not yield detectable TDP-43^{EGFP} recruitment (Figure 2I).

Figure 2. Fluorescently Tagged TDP-43 De-mixes in the Cytoplasm, Forming Liquid-like Droplets that Are Dynamic and Fuse

(A) Schematic of experimental design to assess LLPS properties of cytoplasmic TDP-43 with increasing TDP-43 levels.

(B) U2OS cells expressing high and low levels of cytoplasmic TDP-43$^{\Delta NLS\text{-}Clover}$ and nuclear TDP-43^{mRuby2}.

(C) Relative fluorescence intensity of cytoplasmic TDP-43$^{\Delta NLS\text{-}Clover}$ in cells with (black dots) or without (blue dots) cytoplasmic TDP-43 particles.

(D) Representative fusion and fission events of cytoplasmic TDP-43 liquid-like droplets.

(E) Representative cytoplasmic TDP-43$^{\Delta NLS\text{-}Clover}$ particles (green) formed with increased accumulated levels of TDP-43 in absence of stress (left). FRAP examples of fully (upper panel) or partially (lower panel) bleached TDP-43$^{\Delta NLS\text{-}Clover}$ particles.

(F) Mean fluorescence intensity of the fully bleached TDP-43$^{\Delta NLS\text{-}Clover}$ particle over time, normalized to the average intensity of the particle before photobleaching (and represented as mean ± SEM from the recovery curves of six droplets in a total of three independent experiments). See also Figure S3.

(G) Experimental design to assess LLPS properties of endogenously EGFP-tagged TDP-43 expressed from both endogenous TDP-43 alleles in non-cycling SH-SY5Y cells after incubation with wild-type TDP-43^{mCherry} or FUS^{mCherry} fibrils and visualized over time by live imaging.

(H) Electron micrographs of amyloid-like fibrils of full-length wild-type TDP-43^{mCherry}. Bottom panel illustrates the TDP-43^{mCherry} fibrils after sonication before inoculating them into cell media.

(I) Representative images of neuronal-like SH-SY5Y cells inoculated with sonicated TDP-43^{mCherry} fibrils at a final concentration of 200 nM and further imaged for TDP-43^{mCherry} particles (red) and TDP-43^{EGFP} (green) up to 1 month. Medium was changed every 3 days. Dashed white line outlines nuclei.

(J) Neuronal-like SH-SY5Y cells imaged for direct GFP fluorescence from TDP-43^{EGFP} (green) 1 month after transient incubation with sonicated FUS^{mCherry} particles.

(K) Cytoplasmic droplets of TDP-43^{EGFP} expressed from both endogenous TDP-43 alleles (left). FRAP examples of fully or partially bleached TDP-43^{EGFP} droplets (right).

(L) Mean fluorescence intensity of the fully bleached TDP-43^{EGFP} droplets over time at 10 days or 1 month, normalized to average particle intensity before photobleaching (represented as mean ± SEM from the recovery curves of eight droplets in a total of three independent experiments).

(M) Fusion event between two cytoplasmic TDP-43^{EGFP} droplets. Arrows point to two particles (red and green) that initially fused into one (yellow arrow) at minute 2. At minute 4, another particle (new yellow arrow) fused to the newly formed LLPS at minute 12 (large yellow arrow).

See also Figure S2.

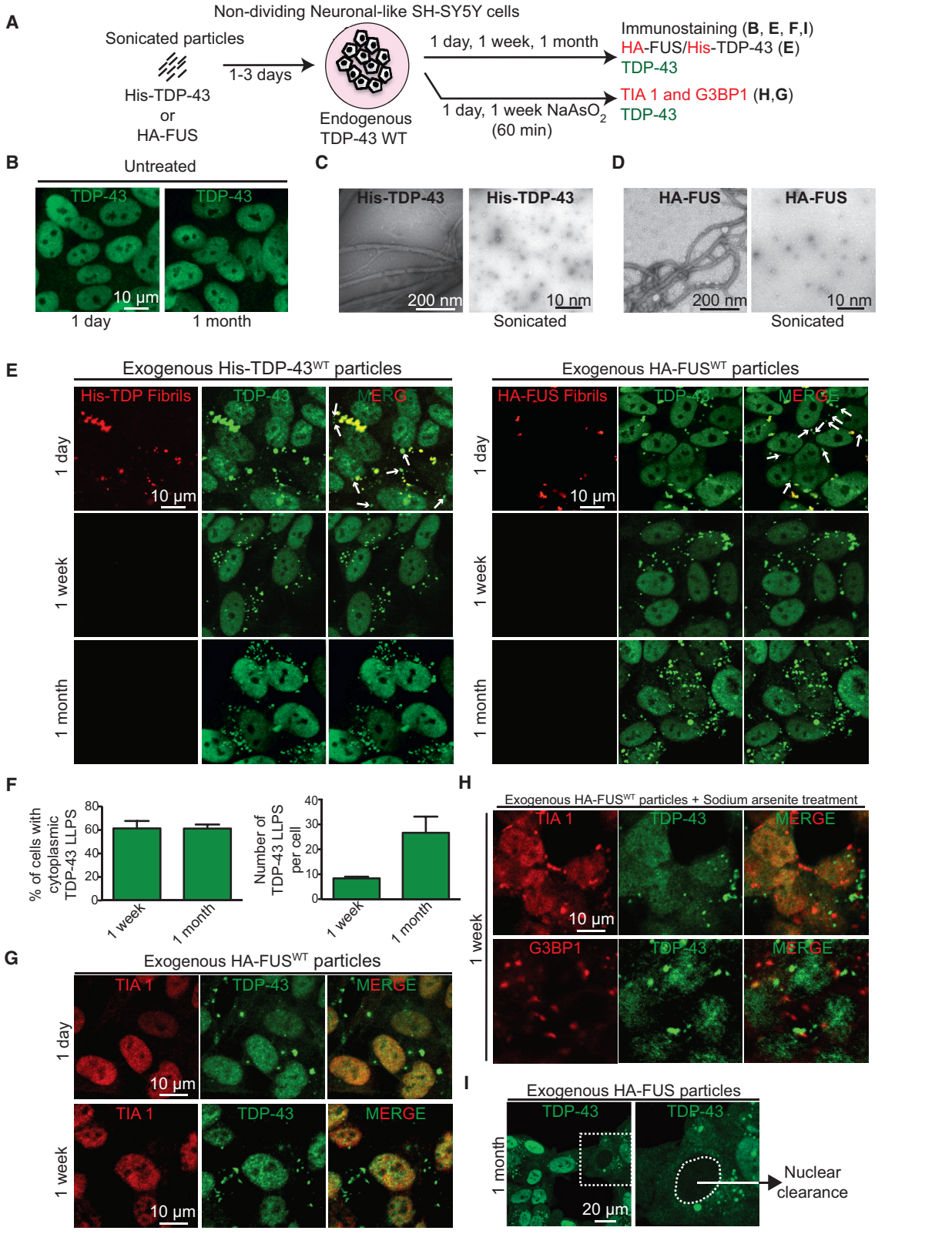

(legend on next page)

However, within 10 days, TDP-43^{EGFP} mislocalized to round, apparently de-mixed cytoplasmic droplets (Figure S2D), and by 1 month, most remaining cells accumulated TDP-43^{EGFP} cytoplasmic particles accompanied by depletion of nuclear TDP-43 (Figure 2I). Cytoplasmic TDP-43 particles were confirmed by immunostaining with TDP-43 antibody (Figure S2E). A parallel experiment with addition of FUS^{mCherry} particles (Figure S2B) yielded almost identical redistribution and apparent de-mixing of TDP-43^{EYFP} expressed at endogenous levels (Figure 2J).

Recovery dynamics after photobleaching were used to determine that 1 month after their induction TDP-43 cytoplasmic particles represented LLPS, with rapid exchange with soluble TDP-43 in the cytoplasm driving fluorescence recovery within 25 s of full or focal photobleaching of single particles (Figures 2K and 2L). Moreover, these old cytoplasmic droplets containing TDP-43 underwent frequent fusion (two examples are shown in Figure 2M) and rarer fission events (Figure S2F), indicative of LLPS. Younger droplets (accumulated 10 days after fibril exposure) displayed ~2.5-fold faster recovery.

Cytoplasmic TDP-43 Liquid De-mixing Independent of Stress Granules

To determine whether endogenous untagged, wild-type TDP-43 can be induced to de-mix in the cytoplasm, we exposed non-dividing neuronal-like SH-SY5Y cells to fragmented TDP-43 or FUS particles (Figures 3A–3D and S3A). Within 24 h, a proportion of initially nuclear TDP-43 (Figure 3E) accumulated in spherical, cytoplasmic particles, many of which (see white arrows, top row, Figure 3E) had undetectable levels of the fragmented TDP-43 or FUS fibrils, respectively. Indeed, no fibril fragments of TDP-43 or FUS could be detected within 4 days after their removal from the media, although in the majority (60%) of cells, a proportion of endogenous TDP-43 remained in a series of round (~1 μm diameter) cytoplasmic particles (Figures 3E and 3F). This apparent de-mixing of TDP-43 was still present a month after fibril exposure, more than 3 weeks after fibrils could no longer be detected (Figure 3E), with the number of apparent droplets increasing 3-fold in a time-dependent manner (Figure 3F). In all cases and time points, TDP-43 remained nuclear and without cytoplasmic particles in untreated cells (Figure 3B) or cells treated with sonicated fragments of fibrils assembled from superoxide dismutase (SOD1) (Figures S3B and S3C).

The cytoplasmic, de-mixed TDP-43 droplets induced by transient exposure to TDP-43 or FUS particles were very different from conventional stress granules, which assemble in response to heat or oxidative stresses and have been proposed to be the crucibles for pathological inclusion formation (Li et al., 2013). With very rare exceptions, no classical stress granule marker (TIA1 and G3BP1) could be detected in fibril-induced TDP-43-containing droplets (Figures 3G and 3H). Further, when stress granules were induced by exposure of the cells to sodium arsenite (Figure S3D), little, if any, endogenously expressed TDP-43 was recruited to the resultant stress granules containing TIA1 or G3BP1 (Figure 3H). Similarly, no stress granule component (e.g., TIA1, Figures S3E and S3F) could be detected in de-mixed, fluorescently tagged TDP-43 (TDP-43^{EGFP}) produced from the endogenous TDP-43 alleles even after cell exposure to arsenite (Figure S3F). Moreover, by 1 month, there was obvious nuclear clearing of TDP-43 in a proportion (~5%) of cells with fibril-induced cytoplasmic TDP-43 particles (Figure 3I), indicating that an external amyloid-like particle-induced re-localization of wild-type endogenous TDP-43 to spherical, cytoplasmic particles can drive loss of nuclear TDP-43 function.

We next followed the kinetics of TDP-43 de-mixing in response to a high (250 μM) dose of sodium arsenite. Conventional stress granules marked by UBAP2L (Figures 4A and 4B) or G3BP1 (Figures 4A and 4D) formed within 20 min and recruited a proportion of an initially diffusely localized cytoplasmic TDP-43$^{\Delta NLS\text{-}Clover}$ (Figure 4B). By 40 min, most cells accumulated stress granules into which a small proportion of TDP-43 was recruited (Figures 4B and 4C). However, by 50 min, new rounded, cytoplasmic assemblies of TDP-43$^{\Delta NLS\text{-}Clover}$ that did not contain UBAP2L began forming (see arrowheads, Figure 4B). By 90 min, most cytoplasmic TDP-43 (including the proportion initially recruited to stress granules) had redistributed into the new cytoplasmic droplets (Figure 4B) in ~90% of the cells (Figure 4C) despite continued presence of arsenite and UBAP2L- or G3BP1-containing stress granules (Figures 4B and 4D). These findings are consistent with observations of recruitment of a small proportion of full-length TDP-43 to stress granules and that this can be enhanced by poly(ADP-ribose) binding to the TDP-43 nuclear-localization sequence (McGurk et al., 2018).

Figure 3. Transient Stress Induces Long-Lasting Untagged, Cytosolic TDP-43 Particles Independent of Conventional Stress Granules

(A) Schematic of experimental design to assess endogenous wild-type TDP-43 de-mixing in the cytoplasm of neuronal-like SH-SY5Y cells (non-cycling).

(B) Representative images of endogenous nuclear TDP-43 in non-fibril-treated SH-SY5Y cells at day 1 (left) and after 1 month of culture (right).

(C and D) Electron micrographs of amyloid-like fibrils of full-length wild-type His-TDP-43 (C) or HA-FUS (D) purified from bacteria. Respective right panels illustrate the His-TDP-43 or HA-FUS fibrils after sonication before inoculating them into cell media.

(E) Representative images of neuronal-like SH-SY5Y cells after 1 day, 1 week, or 1 month after inoculated sonicated His-TDP-43 (left) or HA-FUS (right) fibrils at a final concentration of 200 nM and immunostained with His- or HA-tag (red) and TDP-43 (green) antibodies. Media were changed after 3 days. White arrows indicate cytoplasmic particles containing endogenous wild-type TDP-43 (green).

(F) Left: quantification of the number of cells with cytoplasmic de-mixed TDP-43 over time. Right: quantification of cytoplasmic particles per cell with time (represented as mean ± SEM from 200 cells in a total of three independent experiments).

(G and H) Representative images of SH-SY5Y cells incubated with sonicated HA-FUS particles (G) and immunostained after 1 day (top panel) or 1 week (bottom panel) with stress granule marker TIA1 (red) and TDP-43 (green) antibodies or (H) after treatment with $NaAsO_2$ (0.5 mM) for 1 h and immunostained with TIA1 or G3BP1 (red) and TDP-43 (green) antibodies.

(I) Representative images of SH-SY5Y cells with apparent cytoplasmic TDP-43 de-mixing accompanied by depletion of nuclear TDP-43 1 month post treatment with sonicated HA-FUS particles. Higher magnification of the white boxed area in the left panel (right panel). The white dashed line outlines the nucleus.

See also Figure S3.

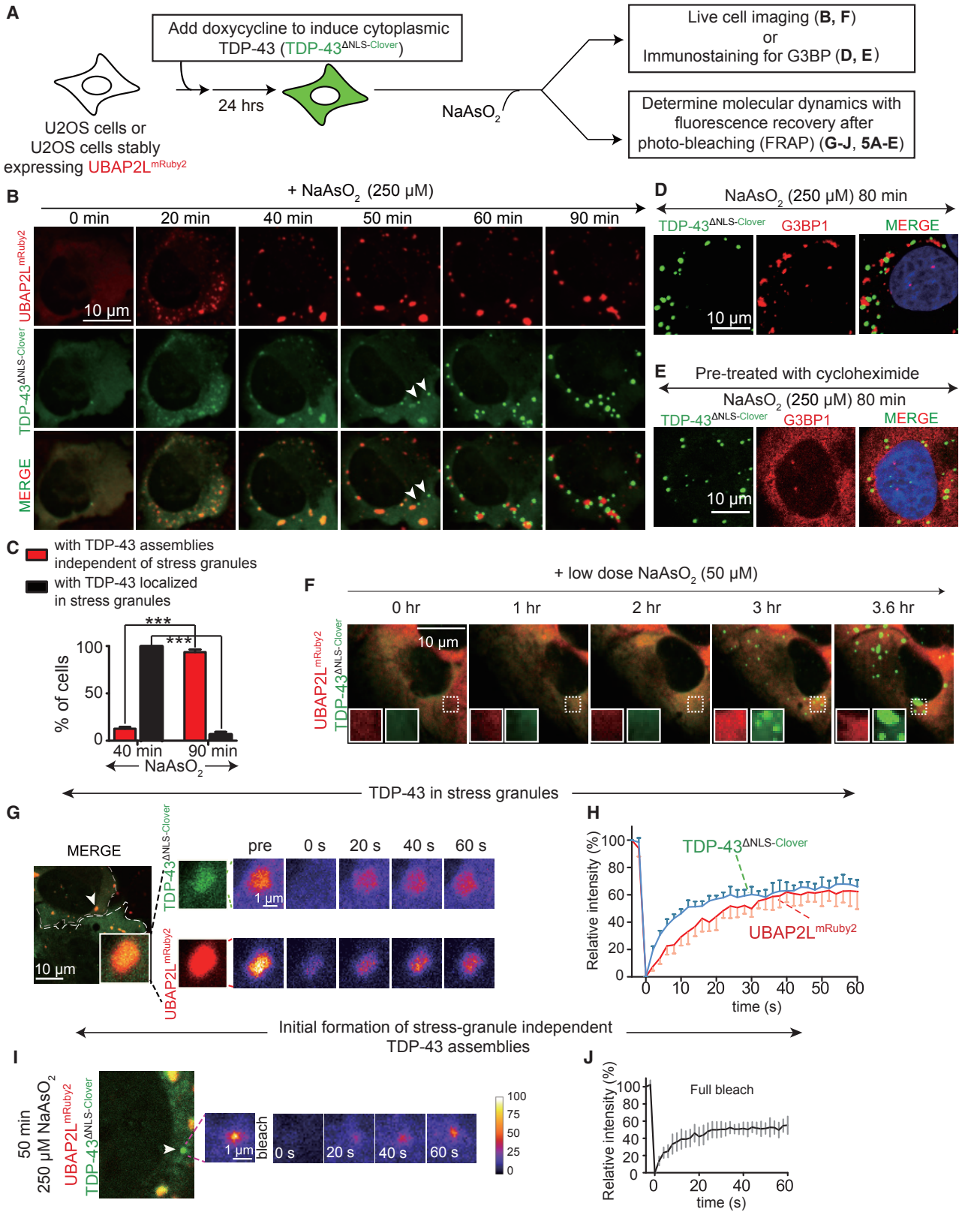

(legend on next page)

Untagged cytoplasmic TDP-43$^{\Delta NLS}$ showed the same apparent arsenite-induced de-mixing behavior without recruitment of stress granule components (Figures S4A and S4B). Furthermore, application of cycloheximide before arsenite treatment abolished stress granule formation (as expected) but had no effect on the timing or extent of TDP-43 assembly into rounded cytoplasmic droplets (Figure 4E). Addition of arsenite to a level too low to induce stress granules still provoked droplets of TDP-43$^{\Delta NLS\text{-}Clover}$ (Figure 4F), consistent with extended low-dose arsenite treatment producing cytoplasmic TDP-43-containing particles that are independent of stress granules and their components (McGurk et al., 2018).

Photobleaching was used to test molecular exchange within the TDP-43 spherical particles that do or do not contain stress granule markers and that formed in the cytoplasm in response to arsenite stress (Figures 4G and 4H). Like UBAP2L itself, about half of the TDP-43 initially recruited into rounded, UBAP2L-positive stress granules recovered rapidly after photobleaching (Figures 4G and 4H), with kinetics similar to the previously reported dynamics of components of conventional stress granules (Molliex et al., 2015). Consistent with droplets formed by LLPS, similarly rapid recovery after photobleaching was seen for about half of the TDP-43 recruited into the rounded TDP-43 assemblies that formed 50 min after exposure to arsenite and that did not contain stress granule components (Figures 4I and 4J).

Arsenite-Induced Gelling of De-mixed Cytoplasmic TDP-43 Droplets

While arsenite-induced stress granules (marked by UBAP2L) maintained liquid properties (Figures 5A and 5B) throughout prolonged arsenite exposure, the initially liquid-like cytoplasmic TDP-43$^{\Delta NLS\text{-}Clover}$ droplets that formed without stress granule components (Figures 4I and 4J) converted within an additional 30 min of arsenite exposure into gels/solids, with almost no intra-particle molecular exchange following partial or complete photobleaching (Figures 5A–5D). The particles did not contain detectable mRNA (Figure S5C), EDC4-containing P body components (Figure S5D), or p62 (Figure S5E) but did acquire TDP-43 phosphorylated at serines 409 and 410 (Figure S5B), as is found in human ALS/FTD pathology. Consistently, the proportion of insoluble TDP-43 increased with time of exposure to arsenite (Figure S5A). Once converted, the particles remained gel/solid-like even after removal of arsenite (Figures 5E and 5F) and recruited p62 with time (Figure S5F).

TDP-43^{EGFP} droplets induced by transient exposure to sonicated fibrils of TDP-43 or FUS remained liquid for at least 3 weeks after initial droplet formation (Figures 2K–2M) without acquisition of amyloid oligomers detectable with the widely used A11 antibody (Figure S5G, left panel) that recognizes a peptide backbone epitope common to amyloid oligomers (Kayed et al., 2007) and also recognizes cytoplasmic TDP-43-containing "myogranules" in regenerating muscle cells (Vogler et al., 2018). However, within 30 min of exposure to sodium arsenite, the TDP-43^{EGFP} droplets quickly converted into a gelled state (Figures 5G and 5H), remaining rounded but with almost no recruitment of new molecules from the cytoplasm after full-particle photobleaching (Figure 5H). Furthermore, 80% of cytoplasmic gel/solid-like TDP-43 particles acquired some amyloid-like character measured with the A11 antibody that recognizes a pre-amyloid oligomeric conformation (Figure S5G, right lower panel). In contrast, almost all of the cytoplasmic TDP-43 de-mixed particles that persisted over 1 month without exposure to arsenite did not acquire detectable amyloid-oligomers (Figure S5G, right upper panel). Hence, arsenite mediates a structural conversion within TDP-43 droplets from weak self-interactions to gels/solids containing β sheet structure, whose incorporation is likely to slow dynamics of exchange with soluble TDP-43 and facilitate TDP-43 aggregation.

TDP-43 De-mixing in iPSC-Derived Motor Neurons Independent of Stress Granules

We next tested whether an increased level of cytoplasmic TDP-43 was sufficient to drive its de-mixing within human motor

Figure 4. Arsenite Induces Cytoplasmic TDP-43 De-mixing into Round, Liquid-like Compartments that Are Distinct from Stress Granules

(A) Schematic of experimental design to assess the relationship of cytoplasmic TDP-43 with stress granules (TDP-43$^{\Delta NLS\text{-}Clover}$) in the presence of sodium arsenite.

(B) Representative images of U2OS cells co-expressing stress granule protein UBAP2L^{mRuby2} and cytoplasmic TDP-43 (TDP-43$^{\Delta NLS\text{-}Clover}$) after addition of 250 μM $NaAsO_2$. White arrowheads indicate round TDP-43 particles independent of stress granules after 50 min of $NaAsO_2$ treatment.

(C) Quantification of TDP-43 recruitment to stress granules and cells that show formation of stress-granule-independent TDP-43 assemblies (from five independent frames in a live-imaging experiment, total cell number from each frame = 25, 12, 30, 16, 10, respectively). Data are shown as box whisker plot (showing mean, min, and max values). ***$p < 0.001$, paired t test.

(D) Endogenous stress granules (using G3BP1 antibody; red) in cells expressing cytoplasmic TDP-43 (TDP-43$^{\Delta NLS\text{-}Clover}$; green) after treatment with $NaAsO_2$ for 80 min.

(E) Endogenous G3BP1 (red) in cells expressing TDP-43$^{\Delta NLS\text{-}Clover}$ (green) after pre-treatment with cycloheximide (10 μg/mL) followed by $NaAsO_2$ treatment for 80 min.

(F) Representative images of U2OS cells co-expressing stress granule protein UBAP2L^{mRuby2} and cytoplasmic TDP-43 (TDP-43$^{\Delta NLS\text{-}Clover}$) after addition of 50 μM $NaAsO_2$.

(G) FRAP of TDP-43$^{\Delta NLS\text{-}Clover}$ (green) and UBAP2L^{mRuby2} (red) in a stress granule.

(H) Mean fluorescence intensity of TDP-43$^{\Delta NLS\text{-}Clover}$ and UBAP2L^{mRuby2} plotted over time (normalized to average intensity of a droplet before photobleaching and represented as mean ± SEM from the recovery curves of a total of four granules from two independent FRAP experiments).

(I) FRAP example of an initial stage formation of a cytoplasmic TDP-43$^{\Delta NLS\text{-}Clover}$ (green) droplet independent of the stress granules UBAP2L^{mRuby2} (red).

(J) Mean fluorescence intensity of TDP-43$^{\Delta NLS\text{-}Clover}$ droplet (indicated by white arrowhead in I) plotted over time (lower graph). Data are normalized to the average intensity of a droplet before photobleaching (and are represented as mean ± SEM from the recovery curves of four droplets in a total of three independent experiments).

See also Figure S4.

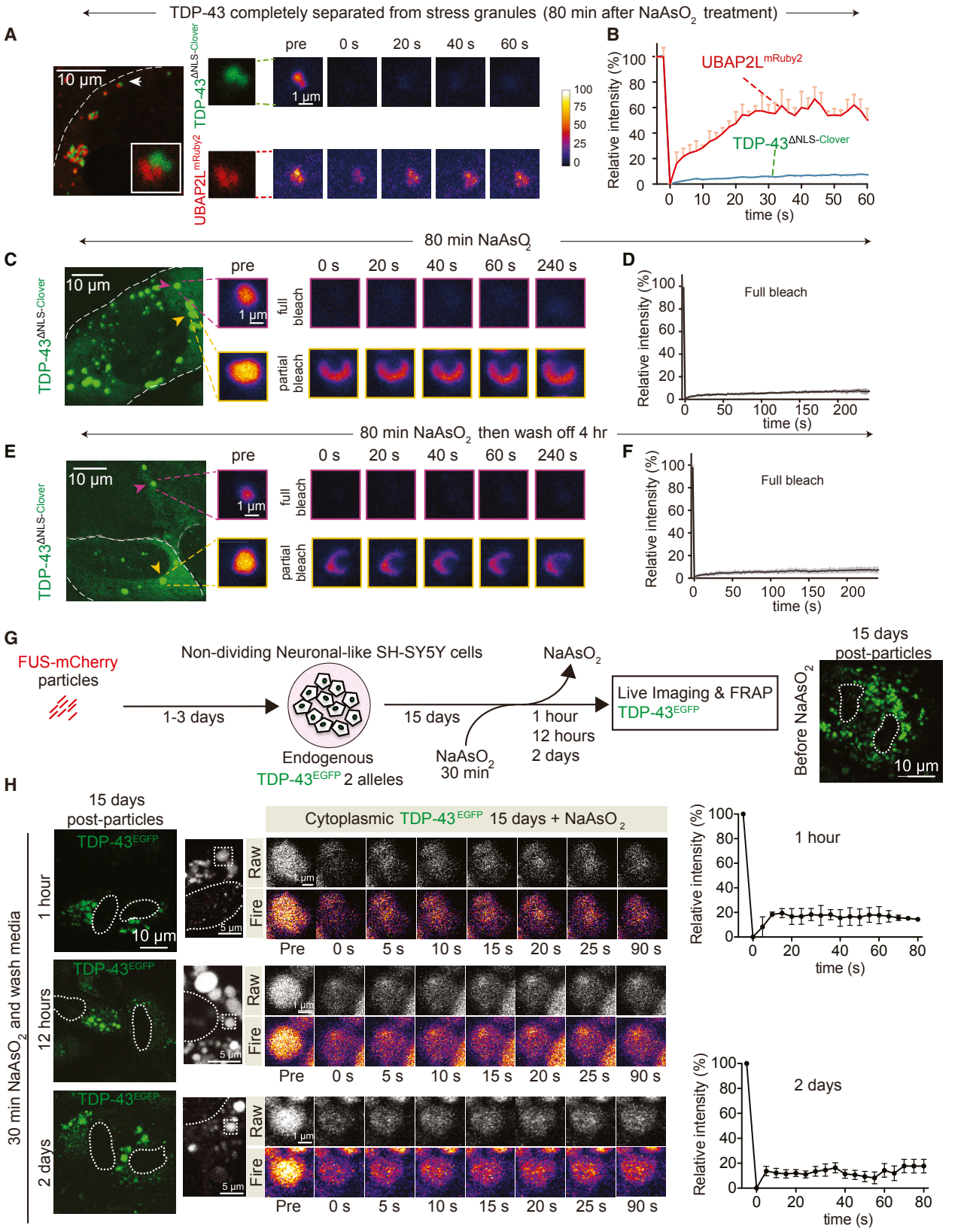

(legend on next page)

neurons (Figure 6A). Forced expression of cytoplasmic TDP-43 in iPSC-derived motor neurons produced rounded cytoplasmic structures in the absence (Figure 6B) or presence of a low dose of sodium arsenite (Figure 6C), in both cases without stress granule assembly or recruitment of stress granule proteins (e.g., G3BP1, Figures 6B and 6C). In the absence of arsenite, the rounded TDP-43 particles were liquid-like (as indicated by fast fluorescence recovery after photobleaching, Figures 6D and 6E). Low-dose arsenite addition rapidly converted the TDP-43-containing droplets into gel/solid-like particles that did not recover after photobleaching (Figures 6F and 6G). Thus, elevation of cytoplasmic TDP-43 level in human motor neurons is sufficient to drive cytoplasmic LLPS of TDP-43 independently of the principal components of stress granules or stress granule assembly.

Cytoplasmic De-mixing Progressively Depletes Nuclear TDP-43 and Induces Cell Death

We next evaluated the kinetics and longevity of cytoplasmic TDP-43 LLPS induced in the cytoplasm by transient exposure to sonicated amyloid-like fibrils and whether continued de-mixing affected cell viability. Fragmented fibrils were transiently added to the culture media of non-cycling, neuronal SH-SY5Y cells genome edited to express TDP-43^{EGFP} from both endogenous TDP-43 alleles (Figure 7A). Within 4 days, TDP-43^{EGFP} partially re-localized into rounded cytoplasmic particles, many of which had undetectable fibrils (e.g., see white arrow, column 2, Figure 7B). The number and size of the cytoplasmic TDP-43-containing particles increased with time (Figures 3F and 7B). Seven days after transient fibril exposure, 50% of the cells had rounded cytoplasmic TDP-43 droplets, but no remaining fibrils could be detected in any cell (Figure 7B). Beginning ~10 days after fibril exposure, cytoplasmic LLPS of TDP-43 was accompanied by nuclear clearing of TDP-43 in some cells. By 1 month, most remaining cells accumulated TDP-43^{EGFP} cytoplasmic particles with nuclear TDP-43 depletion (Figure 7B). The TDP-43 droplets did not contain detectable RNA (Figures S6A, S6B, and S6D) and were independent of arsenite-induced poly-A RNA-containing stress granules (Figure S6C). The 1-month-old cytoplasmic TDP-43 LLPS droplets induced by amyloid-like particles recruited phospho-TDP-43 (Figure 7E), but not ubiquitin or the autophagy adaptor protein p62 (Brady et al., 2011) (Figure S6F). While no cell death was seen within the first week, within 2 weeks after fibril exposure, 60% of cells had died, with most of the remaining cells displaying both cytoplasmic LLPS and nuclear clearance of TDP-43. By 6 weeks, there were almost no cell survivors (Figures 7C and 7D).

Disrupted Nucleocytoplasmic Transport Enhances Nuclear Depletion of TDP-43

Recognizing that defects in nuclear membrane structure and/or nucleocytoplasmic transport have been reported in the nervous systems of patients with ALS caused by hexanucleotide repeat expansion in *C9orf72* (Freibaum et al., 2015; Jovičić et al., 2015; Zhang et al., 2015) or mutation in SOD1 (Kinoshita et al., 2009) and in mouse models of TDP-43 or SOD1 mutant-mediated disease (Chou et al., 2018; Ditsworth et al., 2017; Zhang et al., 2006), we examined the integrity of the nuclear membrane and nuclear import in non-cycling SH-SY5Y neuronal cells with cytoplasmic LLPS of TDP-43. Transient exposure to amyloid-like particles provoked gradual retention in the cytoplasm of components critical for nucleocytoplasmic transport (Figures 8A–8D). Cytoplasmic mislocalization of RanGAP1, the Ran GTPase-activating protein 1 required for Ran-dependent nuclear import and export, was found in some cells within 1 week (Figure 8B). RanGap1 mislocalization increased in a time-dependent manner, with 70% of cells accumulating RanGap1 in large, cytoplasmic inclusions within a month after fibril exposure (Figure 8C), along with progressive accumulation of de-mixed TDP-43 in the cytoplasm.

Imported cargo is released into the nucleus when importin transporters interact with intranuclear Ran-GTP. Correspondingly, high levels of intranuclear Ran-GTP are essential for active transport through nuclear pore complexes (NPCs) and for defining nucleocytoplasmic transport directionality. Consistent with disruption in nuclear import, continuing LLPS of fragmented fibril-induced TDP-43 was accompanied by Ran accumulation into small cytoplasmic inclusions (Figure 8D). Furthermore, after

Figure 5. Arsenite Induces Liquid-Liquid Phase Separation of Cytoplasmic TDP-43 that Quickly Converts into a Gel/Solid State

(A) Representative image using confocal microscopy of TDP-43$^{\Delta NLS\text{-}Clover}$ particles that are independent of UBAP2L^{mRuby2} stress granules after 80 min of $NaAsO_2$ treatment (left). FRAP example of the TDP-43$^{\Delta NLS\text{-}Clover}$ particle (green) and UBAP2L granule (red) shown in the white box (of the left image).

(B) Mean fluorescence intensity of a TDP-43$^{\Delta NLS\text{-}Clover}$ particle and a UBAP2L^{mRuby2} granule plotted over time. Data are normalized to the average intensity of a particle before photobleaching and are represented as mean ± SEM from the recovery curves of five particles in a total of two independent experiments.

(C) Representative of cytoplasmic TDP-43$^{\Delta NLS\text{-}Clover}$ particles (green) after 80 min of $NaAsO_2$ treatment (left). FRAP examples of fully (upper panel) or partially (lower panel) bleached TDP-43$^{\Delta NLS\text{-}Clover}$ particles.

(D) Mean fluorescence intensity of the fully bleached TDP-43$^{\Delta NLS\text{-}Clover}$ particle over time. Data are normalized to the average intensity of a particle before photobleaching and are represented as mean ± SEM from the recovery curves of five particles in a total of two independent experiments.

(E) Representative image of cytoplasmic TDP-43$^{\Delta NLS\text{-}Clover}$ particles (green) after 80 min of $NaAsO_2$ treatment followed by a 4 h wash of arsenite (left). FRAP examples of fully (upper panel) or partially (lower panel) bleached TDP-43$^{\Delta NLS\text{-}Clover}$ particles.

(F) Mean fluorescence intensity of the fully bleached TDP-43$^{\Delta NLS\text{-}Clover}$ particle over time. Data are normalized to the average intensity of a particle before photobleaching and are represented as mean ± SEM from the recovery curves of seven particles in a total of two independent experiments.

(G) Schematic of experimental design to assess LLPS properties of endogenous TDP-43^{EGFP} in cells treated for 2 weeks with FUS particles and sodium arsenite.

(H) Representative images of cytoplasmic endogenous TDP-43^{EGFP} particles after 30 min of sodium arsenite addition in cells treated with FUS particles for 2 weeks (left panel). FRAP examples of TDP-43^{EGFP} particles fully bleached. Mean fluorescence intensity of the fully bleached TDP-43^{EGFP} particles over time (right). Data are normalized to the average intensity of a particle before photobleaching and are represented as mean ± SEM from the recovery curves of four particles in a total of three independent experiments.

See also Figure S5.

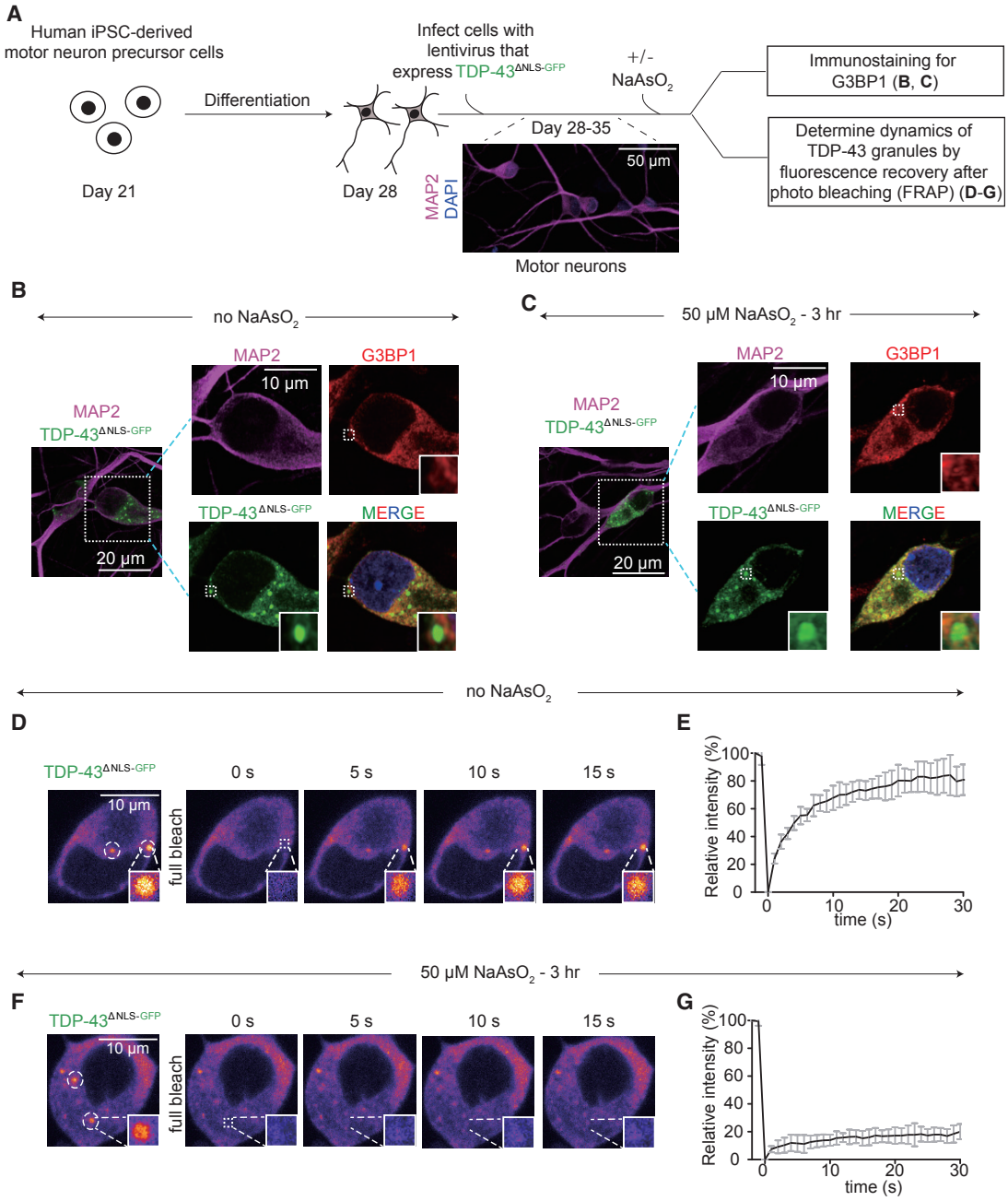

Figure 6. De-mixing of Cytoplasmic TDP-43 in Human iPSC-Derived Motor Neurons Forms Liquid-like Droplets Independent of Stress Granules, which Convert into a Gel/Solid-like State after Arsenite Induced Stress

(A) Schematic of experimental design to assess the properties of de-mixed cytoplasmic TDP-43 particles in human iPSC-derived motor neurons with or without sodium arsenite treatment. Human iPSC-derived motor neuron precursor cells were differentiated for 7 days, and then the differentiated motor neurons were infected with a lentivirus, driving expression of Ubi::TDP-43$^{\Delta NLS\text{-}GFP}$. After 1–2 weeks of expression, the cells were analyzed.

(B and C) Immunostaining of G3BP1 of mature motor neurons expressing cytoplasmic TDP-43 in the absence of sodium arsenite treatment (B) or with 50 µM sodium arsenite (C). MAP2 was stained for neuron marker.

(D and E) Representative images of cytoplasmic TDP-43$^{\Delta NLS\text{-}GFP}$ particles formed in the absence of stress. FRAP example of TDP-43$^{\Delta NLS\text{-}GFP}$ particles in a neuron after a complete bleaching (D). Mean fluorescence intensity of the fully bleached TDP-43$^{\Delta NLS\text{-}GFP}$ particles over time (E). Data are normalized to the average intensity of a particle before photobleaching and are represented as mean ± SEM from the recovery curves of eight particles in a total of four independent experiments.

(F and G) Representative images of cytoplasmic TDP-43$^{\Delta NLS\text{-}GFP}$ particles after 3 h of 50 µM sodium arsenite treatment. FRAP example of TDP-43$^{\Delta NLS\text{-}GFP}$ particles in a motor neuron after a complete bleaching (F). Mean fluorescence intensity of the fully bleached TDP-43$^{\Delta NLS\text{-}GFP}$ particles over time (G). Data are normalized to the average intensity of a particle before photobleaching and are represented as mean ± SEM from the recovery curves of nine particles in a total of four independent experiments.

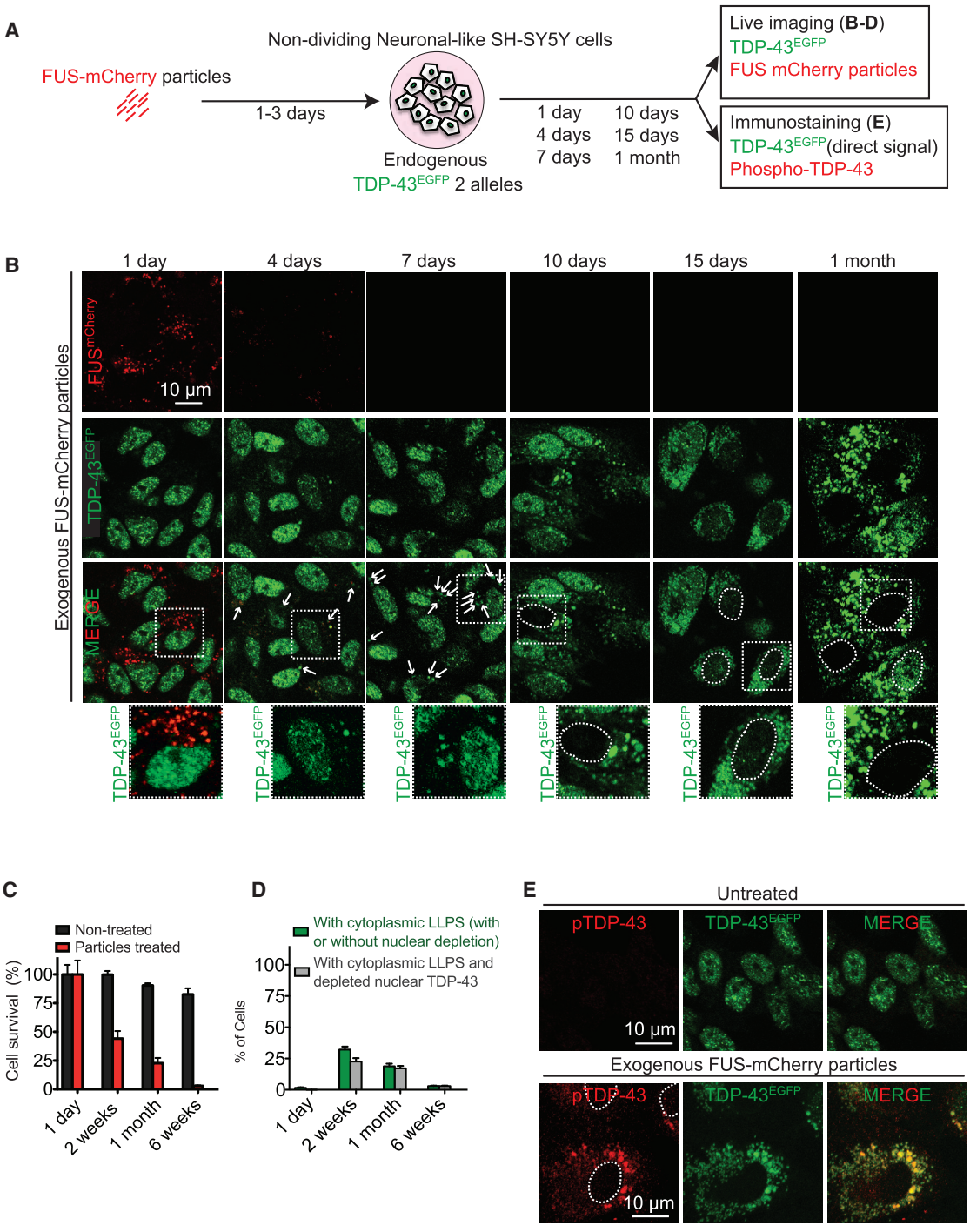

Figure 7. Endogenous EGFP-Tagged TDP-43 De-mixes in the Cytoplasm, Forming Liquid-like droplets that Slowly Deplete Nuclear TDP-43 and Compromise Cell Survival

(A) Schematic of experimental design to assess LLPS properties of endogenously EGFP-tagged TDP-43 in non-cycling SH-SY5Y cells (knockin in both alleles), which were incubated with fluorescently labeled wild-type FUS^{mCherry} fibrils and visualized over time by live imaging or immunofluorescence.

(B) Representative images using confocal microscopy of neuronal-like SH-SY5Y cells inoculated with sonicated His-FUS^{mCherry} particles at a final concentration of 200 nM and further imaged for FUS^{mCherry} fibrils (red) and TDP-43^{EGFP} (green) up to 1 month. Media were changed after 3 days. White arrows indicate cytoplasmic particles containing mislocalized endogenous TDP-43^{EGFP} (green). Dashed white line outlines nuclei.

(C) Cell survival quantification of non-treated (black) and fibril-treated (red) neuronal-like cells over time. Data are represented as mean ± SEM from a total of three independent experiments.

(legend continued on next page)

1 month of TDP-43 LLPS, two components of nuclear pores (Nup107 and Nup62) were found accumulated in cytoplasmic particles, with one (Nup62) co-recruited into rounded TDP-43-containing droplets (see white arrows, Figure 8D), indicative of phase separation of Nup62 together with TDP-43. Similarly, FUS and hnRNPA1 also redistributed to the cytoplasm (Figures S7A and S7B), with hnRNPA1 also recruited into TDP-43 de-mixed particles (Figure S7B, lower panel). The evidence that hnRNPA1 is co-recruited with TDP-43 LLPS is in accordance with a report that the LCD (low complexity domain) of TDP-43 phase separates with the LCD of hnRNPA2 *in vitro* (Ryan et al., 2018). Finally, the nuclear import transporter importin-α, which is not only responsible for recognizing the TDP-43 nuclear localization signal but has also been reported to function as a cytosolic protein chaperone (Jäkel et al., 2002) that together with karyopherin-β1 can dissolve TDP-43 amyloid-like fibrils *in vitro* (Guo et al., 2018), was also phase separated into large, cytoplasmic TDP-43-containing droplets (see white arrows, Figure 8D, lower panels). Overall, induction of cytoplasmic TDP-43 LLPS is sufficient over a timescale of weeks to drive a feedforward mechanism compromising nucleo-cytoplasm transport and exacerbating loss of nuclear TDP-43 (Figure 8E).

DISCUSSION

Here we demonstrate that LLPS reflects a normal TDP-43 behavior *in vivo*, as we show that it is apparently de-mixed intranuclearly in cortical neurons in the mouse brain and multiple examples in cell culture. TDP-43 molecules exhibit fast (within seconds) dynamic exchange within the liquid droplets as well as between the droplets and an aqueous pool. Intranuclear TDP-43 thus recapitulates the characteristics of what has been defined as a liquid produced by LLPS (Boeynaems et al., 2018; Brangwynne et al., 2009). We also show that beyond intranuclear de-mixing, TDP-43 can be induced to de-mix in the cytoplasm (1) when cytoplasmic TDP-43 levels are elevated, (2) in response to transient exposure to amyloid-like fibrillar TDP-43 or FUS, or (3) following exposure to sodium arsenite. In all cases, TDP-43 de-mixes initially into liquid droplets (with rapid molecular exchange with soluble TDP-43 molecules) but converts to rounded gel/solid-like structures with arsenite exposure.

The interaction of TDP-43 (Afroz et al., 2017; Becker et al., 2017; Khalfallah et al., 2018; Li et al., 2013; Ramaswami et al., 2013) or FUS (Guo et al., 2018; Hofweber et al., 2018; Li et al., 2013; Marrone et al., 2018; Zhang et al., 2018) with stress granules has repeatedly been proposed to be a means to enhance their subsequent aggregation. In contrast, we have found that cytoplasmic LLPS of TDP-43 can be independent of components of stress granules and stress granule assembly despite initial recruitment of a small proportion of TDP-43 into stress granules induced with a high dose of sodium arsenite. Perhaps most provocatively, simply increasing cytoplasmic TDP-43 (as would be driven by the known age-dependent reduction in nuclear import; D'Angelo et al., 2009; Mertens et al., 2015) or transient exposure to fibrillar fragments of aggregated TDP-43 (or FUS) recruits TDP-43 into de-mixed cytoplasmic liquid droplets that are independent of stress granules and that slowly deplete nuclear TDP-43 and induce cell death over a 6-week period. Added to the complexity of TDP-43 de-mixing, it is not established whether the cytoplasmic particles we identify here are similar to axonally transported TDP-43-containing droplets that form in cortical neurons following TDP-43 overexpression (Gopal et al., 2017). Identifying the constituents of each of these TDP-43-containing compartments is an unsolved question of high interest for elucidating possible functions carried out within such compartments.

A prominent hallmark of ALS and FTD is nuclear clearance and cytoplasmic TDP-43 aggregation in neurons and glia within the central nervous system (Neumann et al., 2006). Here, we have established that increased TDP-43 concentration in the cytoplasm or application of either of two transient stresses can induce long-lasting LLPS of endogenous TDP-43. While much attention has focused on the relationship of stress granules with disease-related RNA-binding protein aggregation (Becker et al., 2017; Jain et al., 2018; Mackenzie et al., 2017; Markmiller et al., 2018), our findings demonstrate that cytoplasmic de-mixing of TDP-43 can be independent of stress granule formation, with at most a small proportion of TDP-43 transiently recruited to stress granules. Recognizing that other RNA-binding proteins have previously been reported to indirectly associate with TDP-43 through simultaneous binding to a common RNA (Coyne et al., 2015; Elden et al., 2010), it is plausible that transient association of a minority of TDP-43 molecules with stress granules is driven indirectly through TDP-43 binding to RNAs that are also bound to proteins directly recruited to stress granules. In addition, TDP-43 can bind to poly(ADP-ribose) via its nuclear-localization sequence. Binding promotes TDP-43 recruitment to stress granules and delays the initial accumulation of disease-associated TDP-43 phosphorylation that accompanies sustained arsenite-mediated stress (McGurk et al., 2018). TDP-43 phase separation into droplets without conventional stress granule components is consistent with the near absence of evidence using immunohistochemistry and immunofluorescence of stress granule formation or co-localization of stress granule proteins with cytoplasmic TDP-43 aggregates in tissues from patients (Colombrita et al., 2009; Dormann et al., 2010; Liu-Yesucevitz et al., 2010; Mackenzie et al., 2017; McGurk et al., 2014; Neumann et al., 2007) or, more recently, from proteomic analysis of insoluble TDP-43-containing homogenates from ALS or FTD patients (Laferrière et al., 2019).

We have established that transient exposure to amyloid-like TDP-43 (or FUS) particles is sufficient to induce TDP-43 de-mixing into spherical liquid-liquid cytoplasmic droplets (1) that can be stable for weeks and exhibit dynamic internal molecules, (2) that exchange with TDP-43 in the cytoplasm and fusion and fission

(D) Quantification of the percentage of cells with cytoplasmic LLPS (with or without nuclear TDP-43 clearance) (green) or with cytoplasmic LLPS accompanied by nuclear clearance (gray). Data are represented as mean ± SEM from a total of three independent experiments.
(E) Representative images of neuronal-like SH-SY5Y cells 1 month after inoculation of sonicated FUS^{mCherry} fibrils and further immunostained with phospho-TDP-43 (red) and cytoplasmic TDP-43^{EGFP} (green).
See also Figure S6.

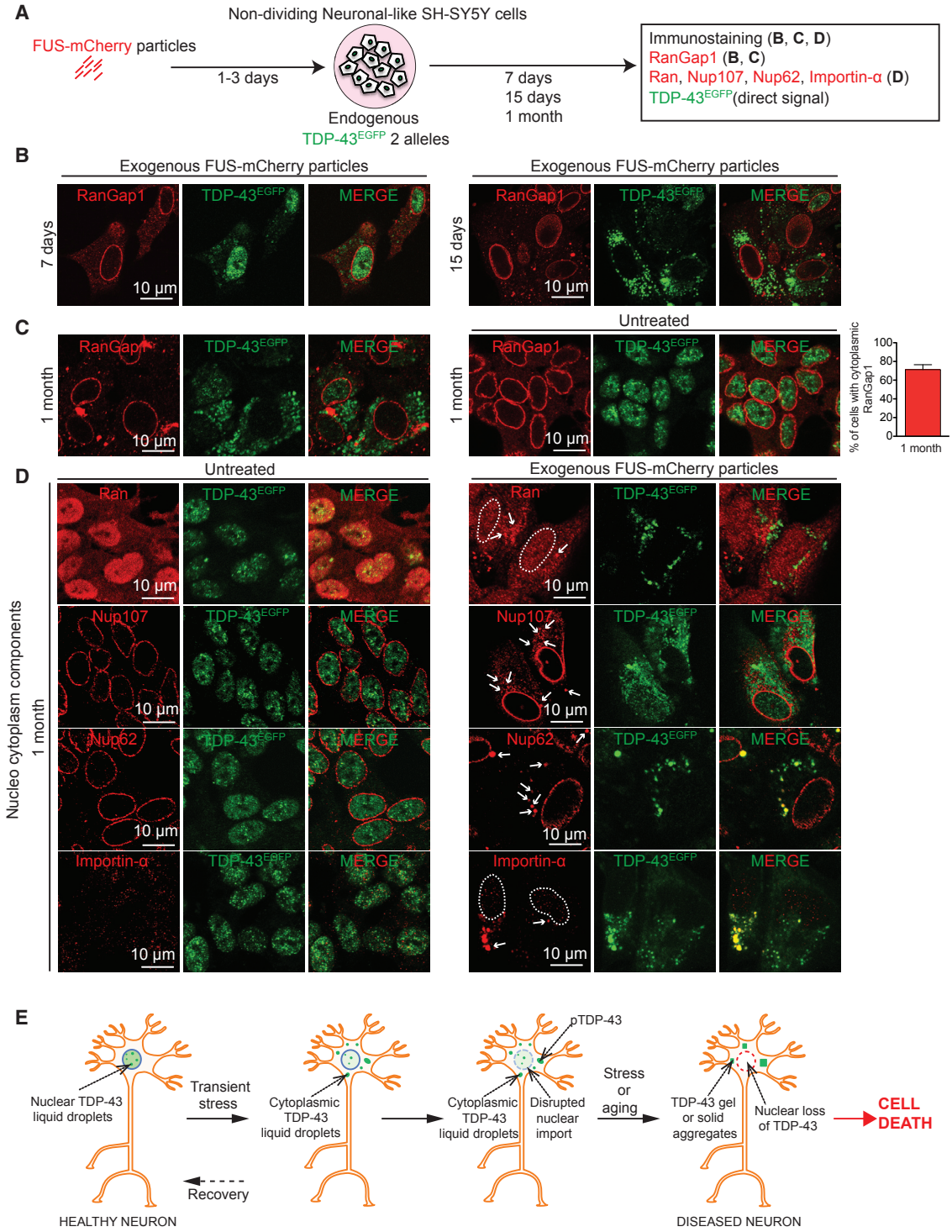

Figure 8. TDP-43 LLPS Is Accompanied by Disruption of Nucleocytoplasmic Transport

(A) Schematic of experimental design to assess LLPS properties of endogenous TDP-43^{EGFP} in cells and their impact on nucleocytoplasmic transport.

(B) Representative images using confocal microscopy of neuronal-like SH-SY5Y cells 7 days and 15 days post incubation of sonicated FUS^{mCherry} fibrils and further immunostained with RanGap1 (red) and cytoplasmic TDP-43^{EGFP} (green).

(C) Immunostained RanGap1 (red) and cytoplasmic TDP-43^{EGFP} (green) 1 month after incubation with FUS^{mCherry} sonicated fibrils (left panel) or in absence of fibril treatment (right panel). Quantification of the percentage of cells with cytoplasmic RanGap1 inclusions 1 month post treatment (from 200 cells in a total of three independent experiments).

(legend continued on next page)

events, and (3) whose presence slowly depletes nuclear TDP-43 accompanied by reduced cell survival. Nuclear TDP-43 depletion has also been reported when TDP-43 is co-recruited into polyglutamine repeat inclusions (Fuentealba et al., 2010). Induced LLPS of TDP-43 is potentially mediated through modifications of it or its binding partners that affect the multivalent interactions that are generally thought to be the driving forces of protein phase separation (Dao et al., 2018; Li et al., 2012; Molliex et al., 2015). Evidence from multiple investigators has supported post-translational modifications and/or binding partners that can act to suppress or enhance de-mixing of FUS (Guo et al., 2018; Hofweber et al., 2018; Qamar et al., 2018; Yoshizawa et al., 2018). Here we show that a portion of TDP-43 within liquid cytoplasmic droplets is phosphorylated, suggesting that LLPS may represent the initial event that then matures to a gel-like solid state that ultimately nucleates TDP-43 aggregation.

A likely, disease-related stress is the reduction in nuclear import during normal aging (D'Angelo et al., 2009; Mertens et al., 2015; Scaffidi and Misteli, 2006), coupled with further import inhibition in different neurodegenerative diseases (Freibaum et al., 2015; Gasset-Rosa et al., 2017), including ALS (Boeynaems et al., 2016; Ditsworth et al., 2017; Freibaum et al., 2015; Jovičić et al., 2015; Zhang et al., 2015, 2018). Here we demonstrate that major regulators of nucleocytoplasmic trafficking (RanGap1, Ran, Nup107, and Nup62) are abnormally localized as a consequence of induced cytoplasmic LLPS of TDP-43. While nuclear-import receptors, including importin-α and karyopherin-β1, have been reported to prevent or reverse TDP-43 aggregation *in vitro* (Guo et al., 2018) (in addition to directly mediating nuclear import of TDP-43), we have found that induced LLPS of TDP-43 in the cytoplasm recruits importin-α, thereby producing an importin-α loss of function that will exacerbate nuclear import deficits. Co-recruitment of Nup62 and importin-α into TDP-43 droplets points to TDP-43 phase separation to be at least one driving force inducing inhibited nuclear import.

We note that reduced nuclear import will obligatorily disrupt the TDP-43 autoregulation pathway (Ayala et al., 2011; Polymenidou et al., 2011), which sets the level of new TDP-43 synthesis through the nuclear action of TDP-43 in the processing of its own pre-mRNA (Polymenidou et al., 2011). Diminished nuclear TDP-43 function, coupled with increased cytoplasmic accumulation from inhibition of nuclear import, produces a feedforward loop for driving increasing cytoplasmic TDP-43 accumulation, further exacerbating the disruption of its autoregulation pathway and producing even higher levels of cytoplasmic TDP-43. During aging, this would be expected to be sufficient to drive concentration-dependent cytoplasmic phase separation of TDP-43, which, together with the loss of TDP-43 nuclear function, ultimately drives cell death.

Lastly, our evidence has shown that beyond age-dependent loss of nuclear import, other stresses—including transient, extracellular contact with aggregated, amyloid-like fibrils of assembled TDP-43 or FUS—can trigger or contribute to the de-mixing of TDP-43 in the cytoplasm. One of these stresses is likely to be a proteome imbalance generated by the altered protein abundances that arise from changes in the levels and/or splicing of >1,500 mRNAs in the nervous system when TDP-43 is diminished (Polymenidou et al., 2011; Tollervey et al., 2011). Efforts to identify additional biological sources of such stress are now of high importance for establishing the cascade of events underlying age-dependent neurodegenerative diseases that have TDP-43 mis-accumulation and aggregation as prominent features.

STAR★METHODS

Detailed methods are provided in the online version of this paper and include the following:

- KEY RESOURCES TABLE
- CONTACT FOR REAGENT AND RESOURCE SHARING
- EXPERIMENTAL MODEL AND SUBJECT DETAILS
  - Mice
  - Cells Lines
- METHOD DETAILS
  - Mice surgery and tissue preservation
  - Immunofluorescence (free-floating OCT-embedded sections)
  - Cell culture
  - Biochemical fractionation of soluble and insoluble proteins
  - Immunoblotting
  - Live cell imaging
  - Fluorescence recovery after photo bleach (FRAP) analysis
  - Immunofluorescence from cells
  - RNA Fluorescence *in situ* hybridization (FISH)
  - SYTO RNA Select Green Fluorescent Cell Stain
  - Recombinant protein purification
  - Amyloid-fibrils reconstruction
  - Transmission Electron Microscopy
  - Survival curve
- QUANTIFICATION AND STATISTICAL ANALYSIS
  - 1. FRAP
  - 2. Cytoplasmic TDP-43 LLPS
  - 3. Fluorescence quantification of Clover in living cells
  - 4. Cell survival and TDP-43 LLPS with nuclear depletion
  - 5. RanGap1 aggregates
  - Statistical Analysis

SUPPLEMENTAL INFORMATION

Supplemental Information can be found with this article online at https://doi.org/10.1016/j.neuron.2019.02.038.

(D) Representative images 1 month post incubation and further immunostained with Ran (upper panel), Nup107 (second panel), Nup62 (third panel), and Importin-α (lower panel) (red) together with cytoplasmic TDP-43^{EGFP} (green). See also Figure S7.
(E) Schematic of how transient stress can induce cytoplasmic TDP-43 LLPS, disruption in nuclear import, accumulation of phospho-TDP-43, conversion from a de-mixed liquid to a gel/solid, depletion with time of nuclear TDP-43, and ultimately cell death.

ACKNOWLEDGMENTS

We would like to thank Mrs. Jennifer Santini (UCSD, Light Microscopy Core) and Mr. Timo Merlo (UCSD, Electron Microscopy Core) for resources. We thank iXCells Biotechnologies for providing human iPSC-derived motor neuron precursor cells. This work was supported by grants from the NIH (R01-NS27036 and P40-NS047101) and the Nomis Foundation. F.G.-R. is the recipient of career development awards from the Muscular Dystrophy Association and Target ALS. H.Y. is recipient of a postdoctoral fellowship from the NIH (F32-AG059358). C.C. received salary support from the ALS Association. Z.M. was recipient of a Human Frontiers Science Program (HFSP) long-term fellowship. D.W.C. and S.D.C. receive salary support from the Ludwig Institute for Cancer Research.

AUTHOR CONTRIBUTIONS

F.G.-R., S.L., H.Y., C.C., S.D.C., and D.W.C. designed the research; F.G.-R., S.L., H.Y., C.C., S.D.C., and D.W.C. analyzed data; F.G.-R., S.L., H.Y., C.C., and Z.M. performed research; F.G.-R. conducted the experiments of fibril-induced cytoplasmic de-mixing of endogenous TDP-43. S.L. conducted the experiments of arsenite-induced TDP-43 de-mixing; F.G.-R., S.L., S.D.C., and D.W.C. wrote the text. L.G. and J.S. provided key reagents.

DECLARATION OF INTERESTS

The authors declare no competing interests.

Received: July 8, 2018
Revised: January 10, 2019
Accepted: February 22, 2019
Published: March 7, 2019

REFERENCES

Afroz, T., Hock, E.M., Ernst, P., Foglieni, C., Jambeau, M., Gilhespy, L.A.B., Laferriere, F., Maniecka, Z., Plückthun, A., Mittl, P., et al. (2017). Functional and dynamic polymerization of the ALS-linked protein TDP-43 antagonizes its pathologic aggregation. Nat. Commun. *8*, 45.

Ayala, Y.M., Zago, P., D'Ambrogio, A., Xu, Y.F., Petrucelli, L., Buratti, E., and Baralle, F.E. (2008). Structural determinants of the cellular localization and shuttling of TDP-43. J. Cell Sci. *121*, 3778–3785.

Ayala, Y.M., De Conti, L., Avendaño-Vázquez, S.E., Dhir, A., Romano, M., D'Ambrogio, A., Tollervey, J., Ule, J., Baralle, M., Buratti, E., and Baralle, F.E. (2011). TDP-43 regulates its mRNA levels through a negative feedback loop. EMBO J. *30*, 277–288.

Becker, L.A., Huang, B., Bieri, G., Ma, R., Knowles, D.A., Jafar-Nejad, P., Messing, J., Kim, H.J., Soriano, A., Auburger, G., et al. (2017). Therapeutic reduction of ataxin-2 extends lifespan and reduces pathology in TDP-43 mice. Nature *544*, 367–371.

Boeynaems, S., Bogaert, E., Van Damme, P., and Van Den Bosch, L. (2016). Inside out: the role of nucleocytoplasmic transport in ALS and FTLD. Acta Neuropathol. *132*, 159–173.

Boeynaems, S., Alberti, S., Fawzi, N.L., Mittag, T., Polymenidou, M., Rousseau, F., Schymkowitz, J., Shorter, J., Wolozin, B., Van Den Bosch, L., et al. (2018). Protein phase separation: a new phase in cell biology. Trends Cell Biol. *28*, 420–435.

Brady, O.A., Meng, P., Zheng, Y., Mao, Y., and Hu, F. (2011). Regulation of TDP-43 aggregation by phosphorylation and p62/SQSTM1. J. Neurochem. *116*, 248–259.

Brangwynne, C.P., Eckmann, C.R., Courson, D.S., Rybarska, A., Hoege, C., Gharakhani, J., Jülicher, F., and Hyman, A.A. (2009). Germline P granules are liquid droplets that localize by controlled dissolution/condensation. Science *324*, 1729–1732.

Burke, K.A., Janke, A.M., Rhine, C.L., and Fawzi, N.L. (2015). Residue-by-residue view of in vitro FUS granules that bind the C-terminal domain of RNA polymerase II. Mol. Cell *60*, 231–241.

Chiti, F., and Dobson, C.M. (2006). Protein misfolding, functional amyloid, and human disease. Annu. Rev. Biochem. *75*, 333–366.

Chou, C.C., Zhang, Y., Umoh, M.E., Vaughan, S.W., Lorenzini, I., Liu, F., Sayegh, M., Donlin-Asp, P.G., Chen, Y.H., Duong, D.M., et al. (2018). TDP-43 pathology disrupts nuclear pore complexes and nucleocytoplasmic transport in ALS/FTD. Nat. Neurosci. *21*, 228–239.

Colombrita, C., Zennaro, E., Fallini, C., Weber, M., Sommacal, A., Buratti, E., Silani, V., and Ratti, A. (2009). TDP-43 is recruited to stress granules in conditions of oxidative insult. J. Neurochem. *111*, 1051–1061.

Cong, L., Ran, F.A., Cox, D., Lin, S., Barretto, R., Habib, N., Hsu, P.D., Wu, X., Jiang, W., Marraffini, L.A., and Zhang, F. (2013). Multiplex genome engineering using CRISPR/Cas systems. Science *339*, 819–823.

Conicella, A.E., Zerze, G.H., Mittal, J., and Fawzi, N.L. (2016). ALS mutations disrupt phase separation mediated by α-helical structure in the TDP-43 low-complexity C-terminal domain. Structure *24*, 1537–1549.

Coyne, A.N., Yamada, S.B., Siddegowda, B.B., Estes, P.S., Zaepfel, B.L., Johannesmeyer, J.S., Lockwood, D.B., Pham, L.T., Hart, M.P., Cassel, J.A., et al. (2015). Fragile X protein mitigates TDP-43 toxicity by remodeling RNA granules and restoring translation. Hum. Mol. Genet. *24*, 6886–6898.

D'Angelo, M.A., Raices, M., Panowski, S.H., and Hetzer, M.W. (2009). Age-dependent deterioration of nuclear pore complexes causes a loss of nuclear integrity in postmitotic cells. Cell *136*, 284–295.

Dao, T.P., Kolaitis, R.M., Kim, H.J., O'Donovan, K., Martyniak, B., Colicino, E., Hehnly, H., Taylor, J.P., and Castañeda, C.A. (2018). Ubiquitin modulates liquid-liquid phase separation of UBQLN2 via disruption of multivalent interactions. Mol. Cell *69*, 965–978.e6.

Ditsworth, D., Maldonado, M., McAlonis-Downes, M., Sun, S., Seelman, A., Drenner, K., Arnold, E., Ling, S.C., Pizzo, D., Ravits, J., et al. (2017). Mutant TDP-43 within motor neurons drives disease onset but not progression in amyotrophic lateral sclerosis. Acta Neuropathol. *133*, 907–922.

Dormann, D., Rodde, R., Edbauer, D., Bentmann, E., Fischer, I., Hruscha, A., Than, M.E., Mackenzie, I.R., Capell, A., Schmid, B., et al. (2010). ALS-associated fused in sarcoma (FUS) mutations disrupt Transportin-mediated nuclear import. EMBO J. *29*, 2841–2857.

Elden, A.C., Kim, H.J., Hart, M.P., Chen-Plotkin, A.S., Johnson, B.S., Fang, X., Armakola, M., Geser, F., Greene, R., Lu, M.M., et al. (2010). Ataxin-2 intermediate-length polyglutamine expansions are associated with increased risk for ALS. Nature *466*, 1069–1075.

Freibaum, B.D., Lu, Y., Lopez-Gonzalez, R., Kim, N.C., Almeida, S., Lee, K.H., Badders, N., Valentine, M., Miller, B.L., Wong, P.C., et al. (2015). GGGGCC repeat expansion in C9orf72 compromises nucleocytoplasmic transport. Nature *525*, 129–133.

Fuentealba, R.A., Udan, M., Bell, S., Wegorzewska, I., Shao, J., Diamond, M.I., Weihl, C.C., and Baloh, R.H. (2010). Interaction with polyglutamine aggregates reveals a Q/N-rich domain in TDP-43. J. Biol. Chem. *285*, 26304–26314.

Gasset-Rosa, F., Chillon-Marinas, C., Goginashvili, A., Atwal, R.S., Artates, J.W., Tabet, R., Wheeler, V.C., Bang, A.G., Cleveland, D.W., and Lagier-Tourenne, C. (2017). Polyglutamine-expanded Huntingtin exacerbates age-related disruption of nuclear integrity and nucleocytoplasmic transport. Neuron *94*, 48–57.e4.

Gopal, P.P., Nirschl, J.J., Klinman, E., and Holzbaur, E.L. (2017). Amyotrophic lateral sclerosis-linked mutations increase the viscosity of liquid-like TDP-43 RNP granules in neurons. Proc. Natl. Acad. Sci. USA *114*, E2466–E2475.

Guo, L., Kim, H.J., Wang, H., Monaghan, J., Freyermuth, F., Sung, J.C., O'Donovan, K., Fare, C.M., Diaz, Z., Singh, N., et al. (2018). Nuclear-import receptors reverse aberrant phase transitions of RNA-binding proteins with prion-like domains. Cell *173*, 677–692.e20.

Hofweber, M., Hutten, S., Bourgeois, B., Spreitzer, E., Niedner-Boblenz, A., Schifferer, M., Ruepp, M.D., Simons, M., Niessing, D., Madl, T., and Dormann, D. (2018). Phase separation of FUS is suppressed by its nuclear import receptor and arginine methylation. Cell *173*, 706–719.e13.

Jain, S., Ba, Z., Zhang, Y., Dai, H.Q., and Alt, F.W. (2018). CTCF-binding elements mediate accessibility of RAG substrates during chromatin scanning. Cell *174*, 102–116.e14.

Jäkel, S., Mingot, J.M., Schwarzmaier, P., Hartmann, E., and Görlich, D. (2002). Importins fulfil a dual function as nuclear import receptors and cytoplasmic chaperones for exposed basic domains. EMBO J. *21*, 377–386.

Johnson, B.S., Snead, D., Lee, J.J., McCaffery, J.M., Shorter, J., and Gitler, A.D. (2009). TDP-43 is intrinsically aggregation-prone, and amyotrophic lateral sclerosis-linked mutations accelerate aggregation and increase toxicity. J. Biol. Chem. *284*, 20329–20339.

Jovičić, A., Mertens, J., Boeynaems, S., Bogaert, E., Chai, N., Yamada, S.B., Paul, J.W., 3rd, Sun, S., Herdy, J.R., Bieri, G., et al. (2015). Modifiers of C9orf72 dipeptide repeat toxicity connect nucleocytoplasmic transport defects to FTD/ALS. Nat. Neurosci. *18*, 1226–1229.

Kayed, R., Head, E., Sarsoza, F., Saing, T., Cotman, C.W., Necula, M., Margol, L., Wu, J., Breydo, L., Thompson, J.L., et al. (2007). Fibril specific, conformation dependent antibodies recognize a generic epitope common to amyloid fibrils and fibrillar oligomers that is absent in prefibrillar oligomers. Mol. Neurodegener. *2*, 18.

Khalfallah, Y., Kuta, R., Grasmuck, C., Prat, A., Durham, H.D., and Vande Velde, C. (2018). TDP-43 regulation of stress granule dynamics in neurodegenerative disease-relevant cell types. Sci. Rep. *8*, 7551.

King, O.D., Gitler, A.D., and Shorter, J. (2012). The tip of the iceberg: RNA-binding proteins with prion-like domains in neurodegenerative disease. Brain Res. *1462*, 61–80.

Kinoshita, Y., Ito, H., Hirano, A., Fujita, K., Wate, R., Nakamura, M., Kaneko, S., Nakano, S., and Kusaka, H. (2009). Nuclear contour irregularity and abnormal transporter protein distribution in anterior horn cells in amyotrophic lateral sclerosis. J. Neuropathol. Exp. Neurol. *68*, 1184–1192.

Laferrière, F., Maniecka, Z., Pérez-Berlanga, M., Hruska-Plochan, M., Gilhespy, L., Hock, E.M., Wagner, U., Afroz, T., Boersema, P.J., Barmettler, G., et al. (2019). TDP-43 extracted from frontotemporal lobar degeneration subject brains displays distinct aggregate assemblies and neurotoxic effects reflecting disease progression rates. Nat. Neurosci. *22*, 65–77.

Li, P., Banjade, S., Cheng, H.C., Kim, S., Chen, B., Guo, L., Llaguno, M., Hollingsworth, J.V., King, D.S., Banani, S.F., et al. (2012). Phase transitions in the assembly of multivalent signalling proteins. Nature *483*, 336–340.

Li, Y.R., King, O.D., Shorter, J., and Gitler, A.D. (2013). Stress granules as crucibles of ALS pathogenesis. J. Cell Biol. *201*, 361–372.

Ling, S.C., Polymenidou, M., and Cleveland, D.W. (2013). Converging mechanisms in ALS and FTD: disrupted RNA and protein homeostasis. Neuron *79*, 416–438.

Liu-Yesucevitz, L., Bilgutay, A., Zhang, Y.J., Vanderweyde, T., Citro, A., Mehta, T., Zaarur, N., McKee, A., Bowser, R., Sherman, M., et al. (2010). Tar DNA binding protein-43 (TDP-43) associates with stress granules: analysis of cultured cells and pathological brain tissue. PLoS ONE *5*, e13250.

Mackenzie, I.R., Nicholson, A.M., Sarkar, M., Messing, J., Purice, M.D., Pottier, C., Annu, K., Baker, M., Perkerson, R.B., Kurti, A., et al. (2017). TIA1 mutations in amyotrophic lateral sclerosis and frontotemporal dementia promote phase separation and alter stress granule dynamics. Neuron *95*, 808–816.e9.

Maharana, S., Wang, J., Papadopoulos, D.K., Richter, D., Pozniakovsky, A., Poser, I., Bickle, M., Rizk, S., Guillén-Boixet, J., Franzmann, T.M., et al. (2018). RNA buffers the phase separation behavior of prion-like RNA binding proteins. Science *360*, 918–921.

Malinovska, L., Kroschwald, S., and Alberti, S. (2013). Protein disorder, prion propensities, and self-organizing macromolecular collectives. Biochim. Biophys. Acta *1834*, 918–931.

Markmiller, S., Soltanieh, S., Server, K.L., Mak, R., Jin, W., Fang, M.Y., Luo, E.C., Krach, F., Yang, D., Sen, A., et al. (2018). Context-dependent and disease-specific diversity in protein interactions within stress granules. Cell *172*, 590–604.e13.

Marrone, L., Poser, I., Casci, I., Japtok, J., Reinhardt, P., Janosch, A., Andree, C., Lee, H.O., Moebius, C., Koerner, E., et al. (2018). Isogenic FUS-eGFP iPSC reporter lines enable quantification of FUS stress granule pathology that is rescued by drugs inducing autophagy. Stem Cell Reports *10*, 375–389.

Mateju, D., Franzmann, T.M., Patel, A., Kopach, A., Boczek, E.E., Maharana, S., Lee, H.O., Carra, S., Hyman, A.A., and Alberti, S. (2017). An aberrant phase transition of stress granules triggered by misfolded protein and prevented by chaperone function. EMBO J. *36*, 1669–1687.

McGurk, L., Lee, V.M., Trojanowksi, J.Q., Van Deerlin, V.M., Lee, E.B., and Bonini, N.M. (2014). Poly-A binding protein-1 localization to a subset of TDP-43 inclusions in amyotrophic lateral sclerosis occurs more frequently in patients harboring an expansion in C9orf72. J. Neuropathol. Exp. Neurol. *73*, 837–845.

McGurk, L., Gomes, E., Guo, L., Mojsilovic-Petrovic, J., Tran, V., Kalb, R.G., Shorter, J., and Bonini, N.M. (2018). Poly(ADP-ribose) prevents pathological phase separation of TDP-43 by promoting liquid demixing and stress granule localization. Mol. Cell *71*, 703–717.e9.

Melamed, Z., López-Erauskin, J., Baughn, M.W., Zhang, O., Drenner, K., Sun, Y., Freyermuth, F., McMahon, M.A., Beccari, M.S., Artates, J.W., et al. (2019). Premature polyadenylation-mediated loss of stathmin-2 is a hallmark of TDP-43-dependent neurodegeneration. Nat. Neurosci. *22*, 180–190.

Mertens, J., Paquola, A.C.M., Ku, M., Hatch, E., Böhnke, L., Ladjevardi, S., McGrath, S., Campbell, B., Lee, H., Herdy, J.R., et al. (2015). Directly reprogrammed human neurons retain aging-associated transcriptomic signatures and reveal age-related nucleocytoplasmic defects. Cell Stem Cell *17*, 705–718.

Mitrea, D.M., and Kriwacki, R.W. (2016). Phase separation in biology; functional organization of a higher order. Cell Commun. Signal. *14*, 1.

Molina-García, L., Gasset-Rosa, F., Álamo, M.M., de la Espina, S.M., and Giraldo, R. (2018). Addressing intracellular amyloidosis in bacteria with RepA-WH1, a prion-like protein. Methods Mol. Biol. *1779*, 289–312.

Molliex, A., Temirov, J., Lee, J., Coughlin, M., Kanagaraj, A.P., Kim, H.J., Mittag, T., and Taylor, J.P. (2015). Phase separation by low complexity domains promotes stress granule assembly and drives pathological fibrillization. Cell *163*, 123–133.

Neumann, M., Sampathu, D.M., Kwong, L.K., Truax, A.C., Micsenyi, M.C., Chou, T.T., Bruce, J., Schuck, T., Grossman, M., Clark, C.M., et al. (2006). Ubiquitinated TDP-43 in frontotemporal lobar degeneration and amyotrophic lateral sclerosis. Science *314*, 130–133.

Neumann, M., Igaz, L.M., Kwong, L.K., Nakashima-Yasuda, H., Kolb, S.J., Dreyfuss, G., Kretzschmar, H.A., Trojanowski, J.Q., and Lee, V.M. (2007). Absence of heterogeneous nuclear ribonucleoproteins and survival motor neuron protein in TDP-43 positive inclusions in frontotemporal lobar degeneration. Acta Neuropathol. *113*, 543–548.

Patel, A., Lee, H.O., Jawerth, L., Maharana, S., Jahnel, M., Hein, M.Y., Stoynov, S., Mahamid, J., Saha, S., Franzmann, T.M., et al. (2015). A liquid-to-solid phase transition of the ALS protein FUS accelerated by disease mutation. Cell *162*, 1066–1077.

Polymenidou, M., Lagier-Tourenne, C., Hutt, K.R., Huelga, S.C., Moran, J., Liang, T.Y., Ling, S.C., Sun, E., Wancewicz, E., Mazur, C., et al. (2011). Long pre-mRNA depletion and RNA missplicing contribute to neuronal vulnerability from loss of TDP-43. Nat. Neurosci. *14*, 459–468.

Qamar, S., Wang, G., Randle, S.J., Ruggeri, F.S., Varela, J.A., Lin, J.Q., Phillips, E.C., Miyashita, A., Williams, D., Ströhl, F., et al. (2018). FUS phase separation is modulated by a molecular chaperone and methylation of arginine cation-π interactions. Cell *173*, 720–734.e15.

Ramaswami, M., Taylor, J.P., and Parker, R. (2013). Altered ribostasis: RNA-protein granules in degenerative disorders. Cell *154*, 727–736.

Rambaran, R.N., and Serpell, L.C. (2008). Amyloid fibrils: abnormal protein assembly. Prion *2*, 112–117.

Rutherford, N.J., Zhang, Y.J., Baker, M., Gass, J.M., Finch, N.A., Xu, Y.F., Stewart, H., Kelley, B.J., Kuntz, K., Crook, R.J., et al. (2008). Novel mutations

in TARDBP (TDP-43) in patients with familial amyotrophic lateral sclerosis. PLoS Genet. *4*, e1000193.

Ryan, V.H., Dignon, G.L., Zerze, G.H., Chabata, C.V., Silva, R., Conicella, A.E., Amaya, J., Burke, K.A., Mittal, J., and Fawzi, N.L. (2018). Mechanistic view of hnRNPA2 low-complexity domain structure, interactions, and phase separation altered by mutation and arginine methylation. Mol. Cell *69*, 465–479.e7.

Scaffidi, P., and Misteli, T. (2006). Lamin A-dependent nuclear defects in human aging. Science *312*, 1059–1063.

Seibenhener, M.L., and Wooten, M.W. (2012). Isolation and culture of hippocampal neurons from prenatal mice. J. Vis. Exp. Published online July 26, 2012. https://doi.org/10.3791/3634.

Sreedharan, J., Blair, I.P., Tripathi, V.B., Hu, X., Vance, C., Rogelj, B., Ackerley, S., Durnall, J.C., Williams, K.L., Buratti, E., et al. (2008). TDP-43 mutations in familial and sporadic amyotrophic lateral sclerosis. Science *319*, 1668–1672.

Sun, Z., Diaz, Z., Fang, X., Hart, M.P., Chesi, A., Shorter, J., and Gitler, A.D. (2011). Molecular determinants and genetic modifiers of aggregation and toxicity for the ALS disease protein FUS/TLS. PLoS Biol. *9*, e1000614.

Taylor, J.P., Brown, R.H., Jr., and Cleveland, D.W. (2016). Decoding ALS: from genes to mechanism. Nature *539*, 197–206.

Tollervey, J.R., Curk, T., Rogelj, B., Briese, M., Cereda, M., Kayikci, M., König, J., Hortobágyi, T., Nishimura, A.L., Zupunski, V., et al. (2011). Characterizing the RNA targets and position-dependent splicing regulation by TDP-43. Nat. Neurosci. *14*, 452–458.

Vogler, T.O., Wheeler, J.R., Nguyen, E.D., Hughes, M.P., Britson, K.A., Lester, E., Rao, B., Betta, N.D., Whitney, O.N., Ewachiw, T.E., et al. (2018). TDP-43 and RNA form amyloid-like myo-granules in regenerating muscle. Nature *563*, 508–513.

Wang, A., Conicella, A.E., Schmidt, H.B., Martin, E.W., Rhoads, S.N., Reeb, A.N., Nourse, A., Ramirez Montero, D., Ryan, V.H., Rohatgi, R., et al. (2018). A single N-terminal phosphomimic disrupts TDP-43 polymerization, phase separation, and RNA splicing. EMBO J. *37*, 37.

Yoshizawa, T., Ali, R., Jiou, J., Fung, H.Y.J., Burke, K.A., Kim, S.J., Lin, Y., Peeples, W.B., Saltzberg, D., Soniat, M., et al. (2018). Nuclear import receptor inhibits phase separation of FUS through binding to multiple sites. Cell *173*, 693–705.e22.

Zhang, J., Ito, H., Wate, R., Ohnishi, S., Nakano, S., and Kusaka, H. (2006). Altered distributions of nucleocytoplasmic transport-related proteins in the spinal cord of a mouse model of amyotrophic lateral sclerosis. Acta Neuropathol. *112*, 673–680.

Zhang, K., Donnelly, C.J., Haeusler, A.R., Grima, J.C., Machamer, J.B., Steinwald, P., Daley, E.L., Miller, S.J., Cunningham, K.M., Vidensky, S., et al. (2015). The C9orf72 repeat expansion disrupts nucleocytoplasmic transport. Nature *525*, 56–61.

Zhang, K., Daigle, J.G., Cunningham, K.M., Coyne, A.N., Ruan, K., Grima, J.C., Bowen, K.E., Wadhwa, H., Yang, P., Rigo, F., et al. (2018). Stress granule assembly disrupts nucleocytoplasmic transport. Cell *173*, 958–971.e17.

STAR★METHODS

KEY RESOURCES TABLE

REAGENT or RESOURCE	SOURCE	IDENTIFIER
Antibodies		
Rabbit anti-TDP-43 (polyclonal)	Proteintech	Cat# 10782-2-AP; RRID: AB_615042
Rabbit anti-TDP-43 (polyclonal)	Proteintech	Cat# 12892-1-AP; RRID: AB_2200505
Mouse anti-GFP (monoclonal, JL-8)	Clontech	Cat# 632381; RRID: AB_2313808
Mouse anti-G3BP1 (monoclonal)	Abcam	Cat# ab56574; RRID: AB_941699
Goat anti-TIA1 (polyclonal)	Santa Cruz	Cat# sc-1751; RRID: AB_2201433
Mouse anti-HA (monoclonal, HA.11)	Covance	Cat# mms-101P; RRID: AB_2314672
Rat anti-tubulin (monoclonal)	Abcam	Cat# ab6160; RRID: AB_305328
Mouse anti-GAPDH (monoclonal)	Abcam	Cat# ab8245; RRID: AB_2107448
Rat anti-phospho-TDP-43	BioLegend	Cat# 829901; RRID: AB_2564934
Goat anti-RanGap1	Santa Cruz	Cat# sc-1862; RRID: AB_2176981
Mouse anti-Ran	BD Bioscience	Cat# bd-610340; RRID: AB_397730
Rabbit anti-Nup107	Abcam	Cat# Ab73290; RRID: AB_1269604
Goat anti-FUS	Bethyl Laboratories	Cat# A303-839A; RRID: AB_2620190
Mouse anti-hnRNPA1	Santa Cruz	Cat# sc-374053; RRID: AB_10947257
Rabbit anti-amyloid A11	Thermo Fisher	Cat# AHB0052; RRID: AB_1501357
Rabbit anti-peIF2a	Cell Signaling	Cat# 3398; RRID: AB_2096481
Guinea pig anti-p62	Progen	Cat# GP62-C; RRID: AB_2687531
Mouse anti-EDC4	Santa Cruz	Cat# sc-376382; RRID: AB_10988077
Mouse anti-ubiquitin	Millipore	Cat# MAB1510; RRID: AB_2180556
Mouse anti-Importin alpha 2	Novus Biologicals	Cat# MAB6207; RRID: AB_10730707
Chicken MAP2	Novus Biologicals	Cat# NB300-213; RRID: AB_2138178
Bacterial and Virus Strains		
E. coli DH 5-alpha competent cells	New England Biolabs	Cat# 2981I
E. coli BL21 competent cells	EMD Millipore	Cat# 69450-3
Chemicals, Peptides, and Recombinant Proteins		
Protamine sulfate	Sigma-Aldrich	Cat# P4020
TransIT-X2 transfection reagent	Mirus	Cat# MIR 6000
Sodium arsenite	Sigma-Aldrich	Cat# 1062771000
PD 0332991 (Palbociclib)	Apexbio	Cat# PD-0332991
Carbonic Anhydrase from bovine erythrocytes	Sigma-Aldrich	Cat# C2273-1VL
Albumin, bovine serum	Sigma-Aldrich	Cat# A8531
B-Amylase from sweet potato	Sigma-Aldrich	Cat# A8781
TEV protease	Thermo Fisher	Cat# 12575015
Poly-D-lysine	Sigma-Aldrich	Cat# P0899
Laminin	Corning	Cat# 354232
20% paraformaldehyde solution, EM grade	Fisher Scientific	Cat# 15713S
Neomycin	Thermo Fisher	Cat# 10131035
Blasticidin	Thermo Fisher	Cat# A1113903
Puromycin Dihydrochloride	Thermo Fisher	Cat# A1113803
Doxycycline	Sigma-Aldrich	Cat# D9891-5G
Uranyl acetate	Ladd R.I., Williston, VT	Cat# 23620
Antibiotic-Antimycotic	Thermo Fisher	Cat# 15240062
Fetal Bovine Serum	Omega Scientific	Cat# FB-01

(*Continued on next page*)

Continued

REAGENT or RESOURCE	SOURCE	IDENTIFIER
Experimental Models: Cell Lines		
iPS Cells	iXCells	N/A
Human: SH-SY5Y	ATCC	Cat# CRL-2266
Human: SH-SY5Y TDP-43$^{AID-GFP}$	This paper	N/A
Human: U2OS	ATCC	Cat# HTB-96
Human: HEK293T	ATCC	Cat# CRL-3216
Experimental Models: Organisms/Strains		
C57BL/6 (C57BL/6 NCrL) mice	Charles River Laboratories	Cat# C57BL/6NCrl
Oligonucleotides		
Synthetic RNA poluCUG repeat (5X)	IDT	N/A
Oligo-dT(20)	Gift from Dr. J. Paul Taylor (St. Jude Children Hospital)	N/A
Recombinant DNA		
pDUET-HA-FUS^{WT}	This paper	N/A
pET His-TDP-43^{WT}	This paper	N/A
pET His-SOD1^{A4V}	This paper	N/A
pRK2- His-FUS^{WT}-mCherry	This paper	N/A
pRK2-His-TDP-43^{WT}-mCherry	This paper	N/A
pRK2-His-TDP-43^{G298S}-mCherry	This paper	N/A
pRK2-His-SOD1^{G93R}-mCherry	This paper	N/A
pX330-U6-Chimeric_BB-CBh-hSpCas9	Addgene Cat# 42230	Cong et al., 2013
Lentivirus		
EF1a-Tet3G-IRES-Neo	This paper	N/A
Ubic-myc-TDP-43^{WT}-mRuby2-SV40-Puro	This paper	N/A
TRE3G-TDP-43$^{\Delta NLS(K82A,R83A,K84A)1-414}$-Clover-EF1acore-BSD	This paper	N/A
Ubic-UBAP2L-mRuby2-SV40-Puro	This paper	N/A
Ubic-TDP-43$^{\Delta NLS(K82A,R83A,K84A)1-414}$-Clover-SV40-Puro	This paper	N/A
pCDH-CMVtet-EYFP-TDP-43	This paper	N/A
Software and Algorithms		
FIJI (ImageJ)	NIH	RRID: SCR_002285; https://fiji.sc/#download
Benchlin webtool	Benchling	https://benchling.com/signup
GraphPad prism	GraphPad	RRID: SCR_002798; https://www.graphpad.com/scientific-software/prism/
Other		
96-well glass bottom plate	Cellvis	Cat# P96-1.5H-N
8-well chamber slides (glass bottom)	Ibidi	Cat# 80827
GSTrap HP columns	GE	Cat# 17-5281-01
HisTrapHP colums	GE	Cat# 7-5248-02
Superdex 75 10/300	GE	Cat# 17-5174-01
Sephadex G-25 in PD-10	GE	Cat# 17-0851-01
Hemacytometer	Fisher Scientific	Cat# 267110
DeltaVision Core system	GE	N/A
Olympus FV1000 Spectral Confocal with SIM Scanner	Olympus	N/A
Tecnai G2 Spirit BioTWIN transmission electron microscope equipped	Tecai	N/A

(*Continued on next page*)

Continued

REAGENT or RESOURCE	SOURCE	IDENTIFIER
Zeiss LSM 880 confocal microscope	Zeiss	N/A
CQ1 confocal quantitative image cytometer	Yokogawa	N/A
SH800S Sony cell sorter	Sony	N/A
JEOL 1200 EX II TEM	JEOL USA	N/A
Akta Pure	GE	N/A
Amaxa Nucleofactor	Lonza	N/A
C-B 300 mesh Cu-01813-F	Ted Pella	Cat# Cu-01813-F

CONTACT FOR REAGENT AND RESOURCE SHARING

Further information and requests for resources and reagents should be directed to and will be fulfilled by the Lead Contact, Don Cleveland: dcleveland@ucsd.edu.

EXPERIMENTAL MODEL AND SUBJECT DETAILS

Mice

C57BL/6 mice were obtained from Charles River Laboratories (Cat# C57BL/6NCrl). Males were perfused in a 4% paraformaldehyde solution and tissues collected for imaging. Maintenance and experimental procedures were approved by the Institutional Animal Care and Use Committee of the University of California, San Diego.

Cells Lines

iPSC-derived motor neurons

Human iPSC cells, derived from peripheral blood mononuclear cells donated by a 58-year-old healthy Caucasian male, were generated by iXCells Biotechnologies and selected for normal karyotype with normal self-renewal and differentiation ability (Melamed et al., 2019). iPS cells were first differentiated into motor neuron precursors in 21 days and then further differentiated into motor neurons for another 7 days using a differentiation protocol patented by iXCells Biotechnologies (Provisional Application no. 14359-001-888) (Melamed et al., 2019). Then the cells were infected by lentivirus to express cytoplasmic TDP-43$^{\Delta NLS\text{-}GFP}$ under ubiquitin promoter as summarized in Figure 6. Human iPSCs were obtained from iXCells and their use further approved by the Embryonic Stem Cell Research Oversight (ESCRO) Committee and Institutional Review Boards (IRB) of the University of California San Diego in accordance with the requirements of the Code of Regulations on the Protection of Human Subjects.

Stable cell line construction: lentivirus infection and selection

HEK293T cells were used for packaging lentiviruses. Briefly, 0.5 x10^6 per well of 293T cells were seeded in a 6-well plate and cultured with DMEM medium (Thermo Fisher) supplemented with 10% FBS (Omega Scientific), 100 units/mL of penicillin, 100 μg/mL of streptomycin, and 250 ng/mL of GIBCO Amphotericin B (Thermo Fisher). For lentiviral transfection, 1.5 μg of the lentiviral plasmid (constructs are labeled as lentivirus in Key Resources Table), 1 μg of pMD2.G and 0.5 μg of psPAX2 were inoculated to each well using Mirus transIT-X2 transfection reagent. Culture medium was changed to fresh medium at 4-24 h post transfection. Two days after transfection, the culture medium was filtered through a 0.45 μm syringe filter to generate the viral soup. The viral soup containing 10-50 μg/mL protamine sulfate was added to U2OS or SH-SY5Y cells cultured in DMEM medium or in DMEM/F12 medium (Thermo Fisher) for infection. The viral soup was removed 24 h after infection, and cells were passaged at least once before selection. Infected cells are selected based on the selection markers encoded by the lentivirus. For U2OS, the concentrations of the antibiotics used for selection were 200 μg/mL for neomycin (Thermo Fisher), 20 μg/mL for blasticidin (Thermo Fisher), 1 μg/mL for puromycin (Thermo Fisher). For SH-SY5Y cells, the concentrations were 400 μg/mL for neomycin, 10 μg/mL for blasticidin and 3 μg/mL for puromycin.

TDP-43 alleles were genetically modified in SH-SY5Y cells. A single guided RNA targeting TDP-43 was designed (Benchlin webtool) and cloned into pSpCas9 plasmid (px330-Addgene) (Cong et al., 2013) using the BbsWE restriction site. The sequence for guided RNA targeting TDP-43 is: GCTGGGGAATGTAGACAGTG. To promote homologous recombination, pSpCas9-gRNA plasmid was electroporated using Amaxa Nucleofactor (assay A-023) along with a template plasmid, containing two TDP-43 homology arms, each 800bp long, separated by AID-GFP segment that is adjacent upstream to the TDP-43 terminal codon. 48 h following electroporation, cells were collected and dissociated using Accutase (Innovative Cell Technologies). GFP-positive cells were sorted and single-cell seeded into 96 wells plates using the SH800S Sony cell sorter. Individual clones were expanded and DNA was extracted for PCR amplification of TDP-43 genomic locus. Insertion of AID-GFP was finally confirmed by immunoblotting. The entire TDP-43 coding region was then sequenced to verify the absence of any additional DNA alteration.

METHOD DETAILS

Mice surgery and tissue preservation

Anesthetized animals (C57BL/6) were subjected to transcardial perfusion with room temperature Sorenson's phosphate buffer (SPB), and fixed with ice-cold 4% paraformaldehyde (PFA) in phosphate buffer (PBS). Brains were removed, trimmed with coronal cuts immediately rostral to the forebrain, post-fixed in 4% PFA for 2 h, cryoprotected in 30% sucrose, embedded in HistoPrep (TM) (SH75-125D, Fisher Chemical) followed by a rapid incubation in −40°C 2-Methylbutane (Fisher Scientific), and kept at −80°C. Fixed brains were cut using the Leica 2800E Frigocut cryostat at −20°C. 35 μm thick free-floating sections were preserved in PBS containing Sodium Azide (0.02%) at 4°C.

Immunofluorescence (free-floating OCT-embedded sections)

The sections were washed in PBS (3 times, 5 min each), permeabilized and blocked in a PBS/0.5% Tween 20/1.5% BSA for 1 h at room temperature, followed by an overnight incubation with the primary antibody anti-TDP-43 (12892-1-AP, Proteintech; 1:500) diluted in a PBS/0.3% Triton X-100 solution at room temperature. Next, sections were washed in PBS (3 times, 10 min each) and incubated with the secondary antibody (diluted in PBS) for 1 h, washed twice with PBS (10 min each), and then incubated for 10 min with PBS/DAPI (Thermo Fisher Scientific, 100ng/mL) solution. Sections were mounted on Fisherbrand Superfrost Plus Microscope Slides (Thermo Fisher Scientific) with ProLong Gold antifade reagent with DAPI (Thermo Fisher Scientific).

Cell culture

All cell lines were cultured at 37°C in a humidified atmosphere at 5% CO_2. U2OS cells were cultured in DMEM (GIBCO) supplemented with 10% fetal bovine serum (FBS) and Antibiotic-Antimycotic (GIBCO). SH-SY5Y cells were cultured in DMEM+F12 (GIBCO) supplemented with 10% FBS and Antibiotic-Antimycotic. When the cell cycle was arrested in G1, Palbociclib (Apexbio) was added into the media. Cell culture media was changed every 3 days.

Primary hippocampal neuronal cultures were prepared as described previously (Seibenhener and Wooten, 2012) with some modifications. In brief, timed pregnant C57BL/6 mice (Charles River) were sacrificed, and embryos were collected at embryonic day 18 (E18). Primary hippocampal neurons were isolated from both male and female embryos and pooled. Cells were dissociated with 0.125% trypsin, and plated on 96-well glass-bottom plates coated with poly-D-lysine (Sigma-Aldrich) at a cell density of 60,000/mL in neurobasal medium (GIBCO) supplemented with 2% B27 (Sigma-Aldrich) and 0.25% glutamine (Sigma-Aldrich). Thereafter, half of the medium was replaced twice a week. Neurons were used 6 to 8 days after plating.

Biochemical fractionation of soluble and insoluble proteins

Cells from six wells were treated as indicated and then lysed in 300 μL of 1x RIPA buffer (50 mM Tris pH 8.0, 150 mM NaCl, 1% NP-40, 5 mM EDTA, 0.5% sodium deoxycholate, 0.1% SDS), supplemented with Halt Protease and Phosphatase Inhibitor Cocktail (Thermofisher). After sonication (13% Amp, 5 s, Branson digital Sonifier), cell lysates were centrifuged at 21,100 × g for 30 min at 4°C and the supernatant was collected as the soluble fraction. The pellet fraction was washed with 1x RIPA buffer once before solubilizing in 75 μL of urea buffer (7M urea, 2 M Thiourea, 4% CHAPS, 30 mM Tris, pH 8.5) and cleared by centrifugation at 21,100 × g for 30 min at 4°C. Then the soluble and insoluble fractions were subsequently analyzed by western blot.

Immunoblotting

Whole-cell extracts (from $5x10^6$cells) were directly lysed in SDS sample buffer and boiled for 10 min. Samples were resolved by SDS–PAGE, transferred to PVDF, and blocked with 5% milk in TBST (TBS, 0.1% Tween-20). The following primary antibodies were used at 1:1,000 dilution (unless noted) in TBST: anti-TDP-43 (10782-2-AP, Proteintech), anti-tubulin (ab6160, Abcam), anti-GFP (632381, Clontech) and 1:2,000 anti-GAPDH (Ab8245, Abcam), anti-phospho-TDP-43 (829901, Biolegend; 1:500). Blots were probed with 1:5,000 dilutions of HRP-conjugated secondary antibodies (GE Healthcare) and exposed to film.

Live cell imaging

U2OS cells were plated on a density of 8,000 cells per well onto a glass-bottom 96-well plate. TDP-$43^{\Delta NLS\text{-}clover}$ proteins were induced for 24 h by adding 1μg/mL of doxycycline. TDP-$43^{\Delta NLS\text{-}clover}$ was induced for 48 h due to the low-level expression of this variant. Live cell imaging was performed on CQ1 Confocal Quantitative Image Cytometer with a 40x objective and environmental control system of 37°C, 95% humidity and 5% of CO_2. Nine z stack images (1 μm per stack) were collected per frame, and the maximum intensity projection was used to construct the final image series. To detect the fast fusion behavior of TDP-43 particles, images were collected at 150 s or 30 s intervals. For sodium arsenite treatment, 0.25 mM or 50 μM of sodium arsenite was added to the cells and images were collected at 2-min, 5-min or 10-min intervals as indicated. A maximal intensity projection image was generated per frame.

SH-SY5Y TDP-43^{EGFP} cells were plated on 8-well chamber (Ibidi) at 25,000 cells per well. After 24 h cells were arrested in G1 with Palbociclib (Apexbio) and maintained arrested during the whole length of the experiment. Sonicated fibrils were added at final

concentration of 200 nM and media was removed after 3 days. Media was changed every 3 days. Live cell imaging was performed on Olympus FV1000 Spectral Confocal (Olympus) at 60x magnification at environmental control system of 37°C, and 5% of CO_2 at the time points indicated.

Fluorescence recovery after photo bleach (FRAP) analysis

FRAP experiments on U2OS cells were performed on Zeiss LSM880 Aryscan microscope with 40x/1.2 W objective. The intensity of the fluorescent signal is controlled in the detection range through changing the laser power, digital gain and off-set. For the green channel, bleaching was conducted by a 488-nm line from an argon laser at ~80%–100% intensity with ~10-20 iterations. FRAP experiments on SH-SY5Y TDP-43^{EGFP} cells were performed on Olympus FV1000 Spectral Confocal using SIM Scanner with 100x oil immersion objective, bleaching was conducted scanning a region of 1x1 μm for 300ms at 8% of laser intensity at 405-nm. Fluorescence recovery was monitored at 0.5 s, 2 s, 5 s or 10 s intervals for 3 min. In the focal-bleach experiment roughly half of a particle is bleached or fully photobleached, and then the distribution of the fluorescence within the photo-manipulated particle is determined over time. During the experiment cells were maintained in Leibovitz's L-15 medium (CO_2 independent).

Immunofluorescence from cells

Primary hippocampal neurons, U2OS and SH-SY5Y cells were cultured on 8-well glass-bottom chamber slides (Ibidi). SH-SY5Y cells were plated on 8-well chamber (Ibidi) at 25,000 cells per well. After 24 h cells were arrested in G1 with Palbociclib (Apexbio) and maintained arrested during the whole length of the experiment. Sonicated fibrils were added at final concentration of 200 nM and media was removed after 3 days. Media was changed every 3 days.

At the indicated time points, cells were fixed with 4% PFA in PBS for 10 min at room temperature After two washes with PBS, cells were permeabilized and blocked with blocking solution (0.1% Triton, 2% BSA in PBS) for 1 h at room temperature. Cells were then incubated overnight with the primary antibody in PBS/0.3% Tween 20. The primary antibodies used for staining were: anti-G3BP1 (ab56574, Abcam; 1:1000), anti-TDP-43 (10782-2-AP, Proteintech; 1:500), anti-TDP-43 (12892-1-AP, Proteintech; 1:500), anti-TIA1 (sc-1751, Santa Cruz; 1:300), anti-HA (mms-101P, Covance; 1:5000), anti-His (H1029, Sigma; 1:2000), anti-RanGap1 (sc-1862, Santa Cruz; 1:500), anti-Ran (bd-610340, BD Bioscience; 1:500) anti-Nup107 (Ab73290, Abcam; 1:300), anti-Nup62 (MABE1043, Millipore; 1:500), anti-FUS (A303-839A, Bethyl Laboratories; 1:500), anti-phospho-TDP-43 (829901, Biolegend; 1:500), anti-hnRNPA1 (sc-374053, Santa Cruz: 1:500), anti-amyloid A11 (AHB0052, ThermoFisher; 1:500), anti-p62 (GP62-C-WBC, Progen; 1:500), anti-EDC4 (sc-376382, Santa Cruz; 1:100) and anti-MAP2 (NB300-213, Novus Biologicals; 1:500). After three washes with PBS, the cells were subsequently incubated with fluorescently labeled secondary antibodies diluted at 1:500 in PBS/0.3% Tween 20 for 1 h at room temperature. After one wash with PBS, one wash with 300 nM DAPWE (PBS) and then one wash with PBS, the cells are preserved in PBS for imaging. SH-SY5Y cells imaging was performed on FV1000 Spectral Confocal (Olympus) at 60-100x magnification.

RNA Fluorescence *in situ* hybridization (FISH)

All hybridization steps were performed under RNase-free conditions. Cells were fixed in 3.7% formaldehyde for 10 min and permeabilized with ethanol 70% for 1 h at 4°C. Then, cells were washed with Wash Buffer (1:5 Wash Buffer A, Biosearch techonolgies Cat SMF-WA1-60 plus 1:10 deionized Formamide) and blocked in the dark at 37°C for 4 h in a humidified chamber with Hybridization Buffer (9:10 RNA FISH Hybridization Buffer Cat SMF-HB1-10 plus 1:10 deionized Formamide) containing 5′-labeled Cy5-(d)T20 oligonucleotides (gift from Dr. J. Paul Taylor, St. Jude Children Hospital) (1ng/μl). After cells were washed with wash buffer in the dark at 37°C for 30 min were stained with DAPI and proceed to imagining.

SYTO RNA Select Green Fluorescent Cell Stain

All the staining steps were performed under RNase-free conditions. SH-SY5Y cells were fixed with cold methanol at −20°C for 10 min and immunostained with anti-TDP-43 (12892-1-AP, Proteintech; 1:500) following the protocol described. Then, cells were washed with PBS two times and stained with freshly prepared RNASelect (Molecular Probes) (500 nM) at room temperature for 20 min. Finally, cells were washed for 5 min in PBS and stained with DAPI.

Recombinant protein purification

All proteins were expressed and purified from *E. colwe* BL21 under native conditions. Protein expression was induced with 1 mM IPTG for 16 h at 16°C. *E.colwe* cells were lysed by sonication on ice in PBS with protease inhibitors (cOmplete, EDTA-free, Roche Applied Science). HA-FUS expression constructs were generated in pGST-Duet to contain a TEV-cleavable site, resulting in GST-TEV-HA-FUS construct. The protein was purified over pre-packed Glutathione Sepharose High Performance resin (GSTrap HP columns, GE) with one-step purification of glutathione S-Transferase (GST) tagged FUS protein using Akta Pure fast protein liquid chromatography (FPLC) system (GE) at 4°C. GST-HA-FUS protein was eluted in 50 mM Tris-HCl, pH 8, 200 mM trehalose, and 20 mM glutathione. His-TDP-43 WT, His-TDP-43$^{WT\text{-}mCherry}$, His-TDP-43$^{G298S\text{-}mCherry}$, His-SOD1$^{WT\text{-}mCherry}$ and His-FUS$^{WT\text{-}mCherry}$ proteins were purified over pre-packed Ni Sepharose High Performance HisTrap HP (GE) using an AKTA pure chromatography system at 4°C and eluted with 50 mM Tris pH 7.4, 100 mM NaCl and 400 mM Imidazole. In the case of His-TDP-43$^{WT\text{-}mCherry}$ Ni-IMAC eluted fractions were followed by gel Filtration Chromatography (Superdex 75 10/300, GE). The following Molecular Weight Markers were

used: Carbonic Anhydrase from bovine erythrocytes (29 KDa, Sigma), Albumin, bovine serum (66KDa, Sigma) and β-Amylase from sweet potato, (200KDa, Sigma). Eluted proteins (GST-HA-FUS, His-TDP-43$^{G298S\text{-}mCherry}$, His-SOD1$^{WT\text{-}mCherry}$ and His-FUS$^{WT\text{-}mCherry}$) with the expected size were collected and concentrated to final concentration of 12 μM using Amicon Ultra centrifugal filter units (10 kDa molecular weight cut-off; Millipore). All proteins after purification were centrifuged for 15 min at 14,000 rpm at 4°C to remove any aggregated material. Protein concentration was calculated by Coomassie Blue with BSA protein as standard, and by colorimetric Bradford assay (Bio-Rad). For protein storage at −80°C glycerol was added (30%)

Amyloid-fibrils reconstruction

HA-FUS^{WT} protein was buffer exchanged at 4°C into FUS assembly buffer (50 mM Tris-HCl, pH 8, 200 mM trehalose, 1 mM DTT, 20 mM glutathione). Seed formation was initiated by addition of TEV protease to GST-TEV-HA-FUS (4 μM) in FUS assembly buffer for 3 h and then high salt storage buffer (40 mM HEPES pH7.4, 500 mM KCl, 20 mM MgCl2, 10% glycerol, 1 mM DTT) was added for 3 h (Sun et al., 2011). FUS fibrilization was initiated by adding 1:20 of FUS seeds to GST-TEV-FUS (4 μM) and TEV protease in FUS assembly buffer for 24 h at 22°C. The fibrils generated were sonicated at 45% for 45 s. Sonicated fibrils were used as seeds on the following FUS fibrilization assays. His-FUS^{mCherry} was initially dialyzed with FUS$^{WT\text{-}mCherry}$ assembly buffer (Tris 50 mM pH 7.4, 100 mM NaCl, 1 mM DTT). Fibrils were generated by adding sonicated HA-FUS^{WT} fibrils to His-FUS$^{WT\text{-}mCherry}$ (4 μM) for 24 h at 22°C.

His-TDP-43 protein (4 μM) was initially dialyzed at 4°C with Tris 50 mM pH 7.4, 100 mM NaCl, 1 mM DTT buffer. Fibrils were induced by adding polyethylene glycol (PEG)-4000 (7%) and 2-methyl-2,4-pentanediol (MPD) (3%) for 16 h at 22°C. Sonicated His-TDP-43 fibrils were used as seeds on the following TDP-43 fibrilization assays. His-TDP-43$^{WT\text{-}mCherry}$ fibrils were generated by adding sonicated His-TDP-43 fibrils as seeds to soluble His-TDP-43$^{WT\text{-}mCherry}$ in TDP-43 assembly buffer supplemented with 7% PEG and 3% MPD.

His-SOD1$^{G93A\text{-}mCherry}$ fibrilization was induced by adding SOD1^{A4V} aggregates produced in bacteria. Briefly, SOD1^{A4V} protein aggregates were induced in BL21 cells, bacteria cell pellet was collected, lysed, and centrifuged/resuspended for 5 cycles (Molina-García et al., 2018). Then a sucrose discontinuous gradient was prepared: in a 2 mL Eppendorf tube, successively was displayed 200 μL of 60 (bottom)> 50 > 40 > 30 > 20% (top) sucrose, freezing each layer at −80°C before adding the next one. Resuspended aggregates were laid on the sucrose gradient and centrifuged at 10,000 rpm 1 h at 4°C. Fractions were carefully collected and a Coomassie Blue gel was performed to identify the fraction(s) that contained SOD1^{A4V} protein. SOD1^{A4V} containing fractions were further dialyzed with PBS and sonicated. The final product was used as seeds for His-SOD1$^{G93A\text{-}mCherry}$ fibrilization. Seeds were added to His-SOD1$^{G93A\text{-}mCherry}$ (4 μM) in SOD1 assembly buffer (100 mM Na_2SO_4, 30 mM Tris–HCl pH 8, 4 mM $MgSO_4$, 7% polyethylene glycol (PEG)-4000 and 3% 2-methyl-2,4-pentanediol (MPD)) at 22°C during 16 h. Finally, fibrils were dialyzed using slide-A-Lyzer MINWE Dialysis Units (10 kDa molecular weight cut-off; Thermo) in PBS for 3 h and sonicated at 45% 45 s just before adding them to the cell media.

Transmission Electron Microscopy

Fibril protein reactions (10 μl) were adsorbed onto glow-discharged 300-mesh Formvar/carbon coated copper grids (Ted Pella) and stained with 2% (w/v) aqueous uranyl acetate (Ladd Research Industries, Williston, VT). Excess liquid was removed, and grids were allowed to air dry. Grids were examined using a Tecnawe G2 Spirit BioTWIN transmission electron microscope equipped with an Eagle 4k HS digital camera (FEI, Hilsboro, OR).

Survival curve

For survival curve analysis, SH-SY5Y TDP-43^{EGFP} cells were plated on a 24 well-plate and cytoplasmic LLPS were induced with His-FUS^{mCherry} fibrils as described. At indicated time points, cells were collected and counted using a haemocytometer (Fisher Scientific).

QUANTIFICATION AND STATISTICAL ANALYSIS

All quantitative analyses relied on systematic uniform random sampling.

1. FRAP

The FRAP data were quantified using ImageJ. The time series of the granule fluorescence intensity was calculated and the intensity of the background (area with no cells) was subtracted from the granule intensity. The intensity of the granule during the whole experiment was normalized to one before bleaching and the intensity of the granule just after bleaching was normalized to zero. An average of at least 4-20 particles per condition was used to calculate the mean and standard deviation. The averaged relative intensity and standard error were plotted to calculate the dynamics of the particles.

2. Cytoplasmic TDP-43 LLPS

Number of cells with cytoplasmic TDP-43 particles and number of cytoplasmic particles were counted on 60x images taken on the Olympus FV1000 Spectral Confocal. DAPI staining was used to address cytoplasmic localization. ~200 cells were counted per condition and time point. Quantification was performed in at least three independent replicates. Arsenite induced cytoplasmic TDP-43

de-mixing was done using live cell imaging on CQ1 Confocal Quantitative Image Cytometer with a 40x objective and environmental control system of 37°C, 95% humidity and 5% of CO_2. Quantification of the cells was done on five independent videos at the corresponding time point with a total number of 93 cells.

3. Fluorescence quantification of Clover in living cells

U2OS were plated on 8-well glass-bottom chamber slides (Ibidi). Imaging of TDP-$43^{\Delta NLS\text{-}clover}$ were done using the 20x objective (0.8. air. 0.55 mm) on Zeiss LSM880 confocal microscope with settings: scan resolution = 1024 × 1024; scan speed level = 8; pinhole = 20; Gain was set at 500 and offset was set to 600 so that all the signal was in the linear range. 488 nm were used for excitation and the signals from 500 nm to 600 nm were collected. Mean intensity of TDP-$43^{\Delta NLS\text{-}clover}$ in the cytoplasm was measured using FIJI (ImageJ) by circling the area of the cells with fluorescence. Dot plotting of the intensity from 23 cells with TDP-43 granules, and 27 cells without granules from nine images.

4. Cell survival and TDP-43 LLPS with nuclear depletion

Cell survival was quantified manually with using a haemocytometer. The number of survival cells was normalized to day 1 post-fibril treatment. Non-fibrils treated cells were added as control. Survival was measured in at least three independent replicates.

Quantifications of the percentage of cells with cytoplasmic LLPS (with or without nuclear TDP-43 clearance), or with cytoplasmic LLPS accompanied by nuclear clearance were quantified manually on 60x images taken on the Olympus FV1000 Spectral Confocal. DAPI staining was used to address cytoplasmic localization. Data are represented as mean ± SEM from a total of three independent experiments.

5. RanGap1 aggregates

Number of cells with cytoplasmic RanGap1 aggregates were counted manually on 60x images taken on the Olympus FV1000 Spectral Confocal. 200 cells were counted. Quantification was performed in at least three independent replicates.

Statistical Analysis

Statistical analyses were performed using GraphPad Prism. All data are shown as the box whisker plot (mean, min, and max value) or mean ± standard error of the mean (SEM). The statistical significance of the differences between two groups was investigated by paired t test. Statistical tests are indicated in each figure legend along with the corresponding significance level (p value). The number of cells analyzed per experiment is provided in the corresponding figure legends.

Neuron, Volume *102*

Supplemental Information

Cytoplasmic TDP-43 De-mixing Independent of Stress Granules Drives Inhibition of Nuclear Import, Loss of Nuclear TDP-43, and Cell Death

Fatima Gasset-Rosa, Shan Lu, Haiyang Yu, Cong Chen, Ze'ev Melamed, Lin Guo, James Shorter, Sandrine Da Cruz, and Don W. Cleveland

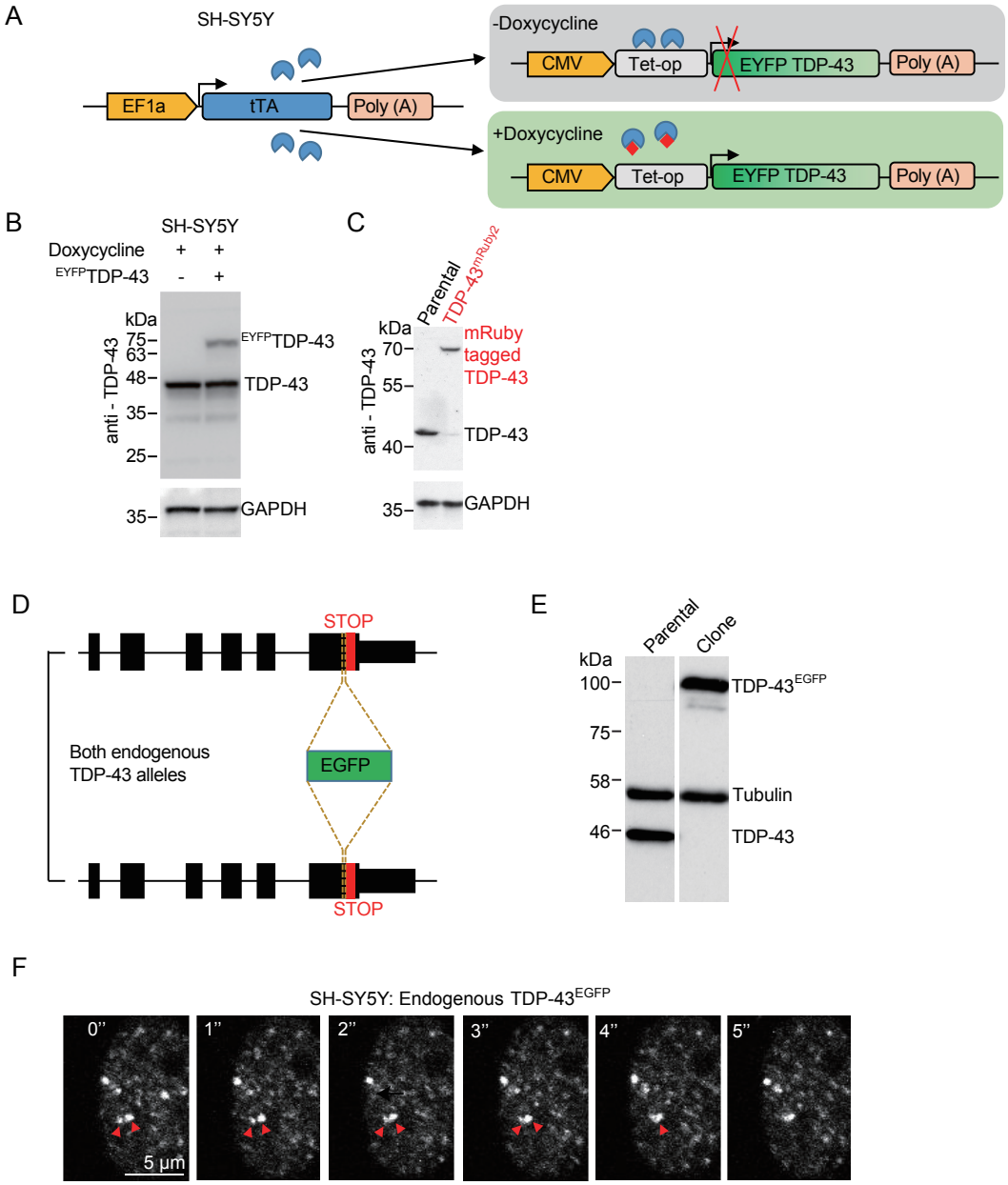

Figure S1: Expression of fluorescently-tagged TDP-43 at physiological levels in SH-SY5Y cells. (Related to Figure 1) (A) Scheme outlining doxycycline inducible expression of TDP-43 with N-terminally tagged EYFP (^{EYFP}TDP-43) in SH-SY5Y cells. (B) Immunoblot showing ^{EYFP}TDP-43 levels in SH-SY5Y cells after 72 hours of induction using a TDP-43 antibody. GAPDH antibody was used as loading control. (C) Immunoblotting of TDP-43 levels in U2OS cells expressing TDP-43^{mRuby2} upon doxycycline induction compared to endogenous TDP-43. GAPDH was used as loading control. (D) Scheme illustrating the genome editing of TDP-43 locus to introduce AID-EGFP in both TDP-43 alleles before the stop codons in SH-SY5Y cells. (E) Immunoblot showing that TDP-43$^{AID-EGFP}$ replaces endogenous TDP-43 with TDP-43 total level being maintained (compared to the parental untagged cells) using TDP-43 antibody. Tubulin antibody was used as loading control. (F) Representative fusion event of endogenous TDP-43^{EGFP} droplets in SH-SY5Y cells. Red arrowheads indicate the fusing droplets.

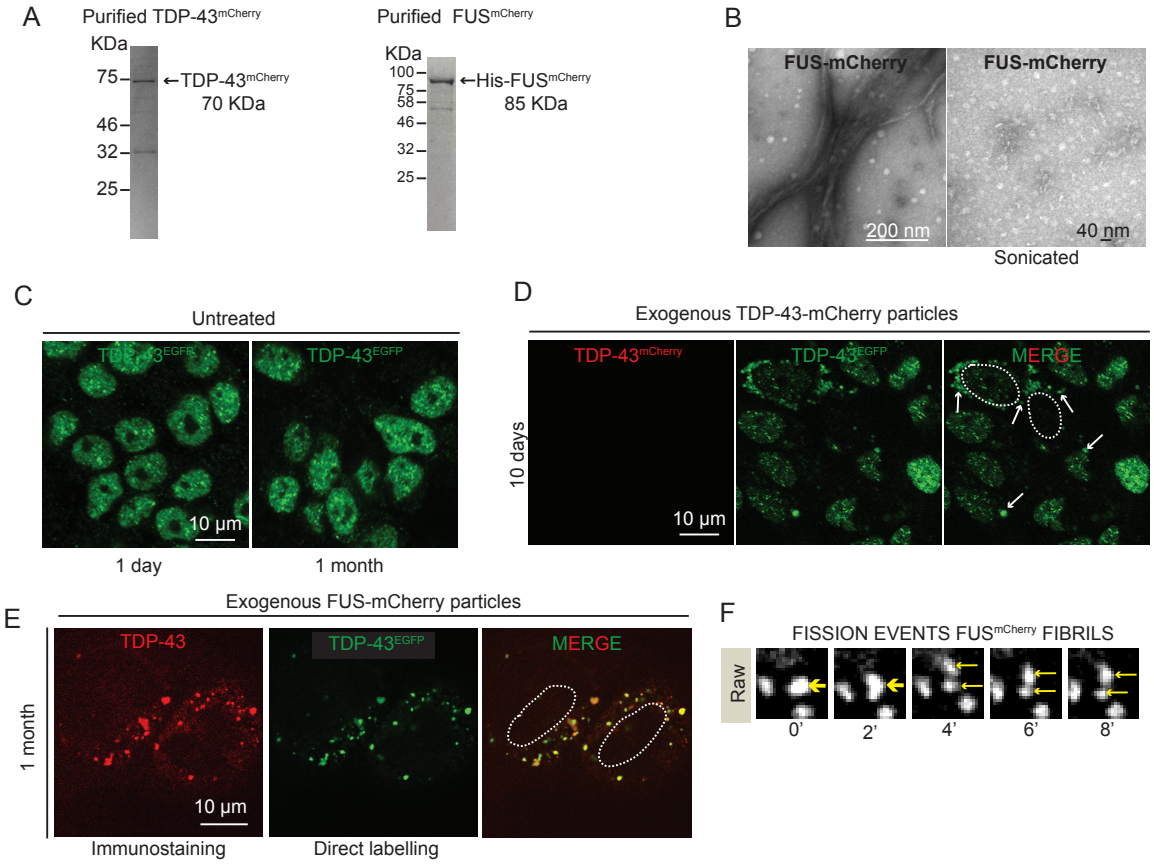

Figure S2: After 10 days of TDP-43^{mCherry} particles treatment, TDP-43 mislocalizes in the cytoplasm and TDP-43 LLPS presents fission events. (Related to Figure 2) (A) Coomassie blue staining of recombinant TDP-43^{mCherry} protein purified from bacteria at the expected size of 70 KDa (left panel), and FUS^{mCherry} protein at the expected size of 85 KDa (right panel). (B) Electron micrograph of amyloid-like fibrils of FUS^{mCherry} recombinant protein purified from bacteria. Right panel illustrates the FUS^{mCherry} fibrils after sonication before inoculating them into cell media. (C) Representative images using confocal microscopy of endogenous nuclear TDP-43^{EGFP} in non-fibril-treated SH-SY5Y cells at day 1 (left) and after 1 month of culture (right). (D) Representative images using confocal microscopy of neuronal-like SH-SY5Y cells inoculated with sonicated His-TDP-43^{mCherry} particles at a final concentration of 200 nM and further imaged for TDP-43^{mCherry} fibrils (red) and TDP-43^{EGFP} (green) at 10 days. Media was changed after 3 days. White arrows indicate cytoplasmic particles containing mislocalized endogenous TDP-43^{EGFP} (green). Dashed white line outlines nuclei. (E) Representative images using confocal microscopy of neuronal-like SH-SY5Y cells inoculated with sonicated FUS^{mCherry} fibrils and immunostained with TDP-43 antibody (red) with direct GFP fluorescence signal from TDP-43^{EGFP} (green). (F) A representative fission event of cytoplasmic TDP-43^{EGFP} LLPS is shown with thick yellow arrow pointing to the particle that is divided into two new particles (two thinner arrows) at minute 4.

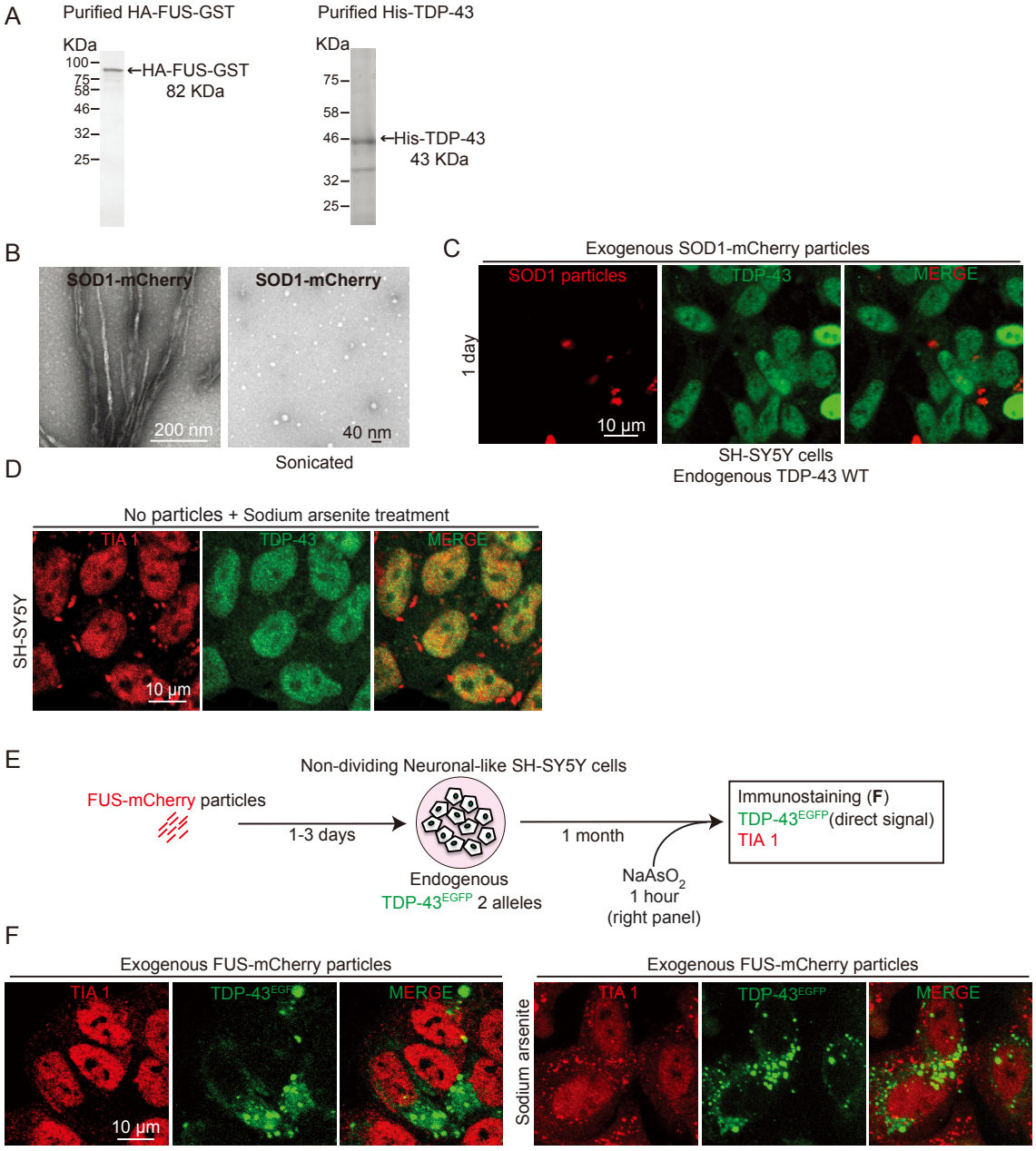

Figure S3: TDP-43 droplets are induced by FUS particles, but not SOD1 particles and are independent of stress granules. (Related to Figure 3) (A) Coomassie blue staining of recombinant HA-FUS-(TEV cleavage site)-GST protein purified from bacteria at the expected size of 82 KDa (left panel), and His-TDP-43 protein at the expected size of 43 KDa (right panel). (B) Electron micrograph of amyloid-like fibrils of $SOD1^{mCherry}$ recombinant protein purified from bacteria. Right panel illustrates the $SOD1^{mCherry}$ fibrils after sonication before inoculating them into cell media. (C) Representative images using confocal microscopy of neuronal-like SH-SY5Y cells inoculated with sonicated $SOD1^{mCherry}$ particles (red) and immunostained after 1 day TDP-43 antibody. D) Confocal representative images of neuronal-like cells treated with $NaAsO_2$ (500 mM) for 1 hour and immunostained with TIA1 (red) and TDP-43 (green) antibodies to induce TIA1 positive stress granules. (E) Scheme of the experimental design to assess stress granule dependency of endogenously EGFP tagged TDP-43 in non-cycling SH-SY5Y cells (knock-in in both alleles), which were incubated with fluorescently labelled $FUS^{mCherry}$ particles and visualized over time by live-imaging or immunofluorescence. (F) Representative images using confocal microscopy of neuronal-like SH-SY5Y cells inoculated with sonicated $FUS^{mCherry}$ particles in absence (left panel) or presence of $NaAsO_2$ for 1 hour (right panel) and further immunostained with stress granules marker TIA1 (red) and cytoplasmic $TDP\text{-}43^{EGFP}$ (green) after 1 month of fibril treatment.

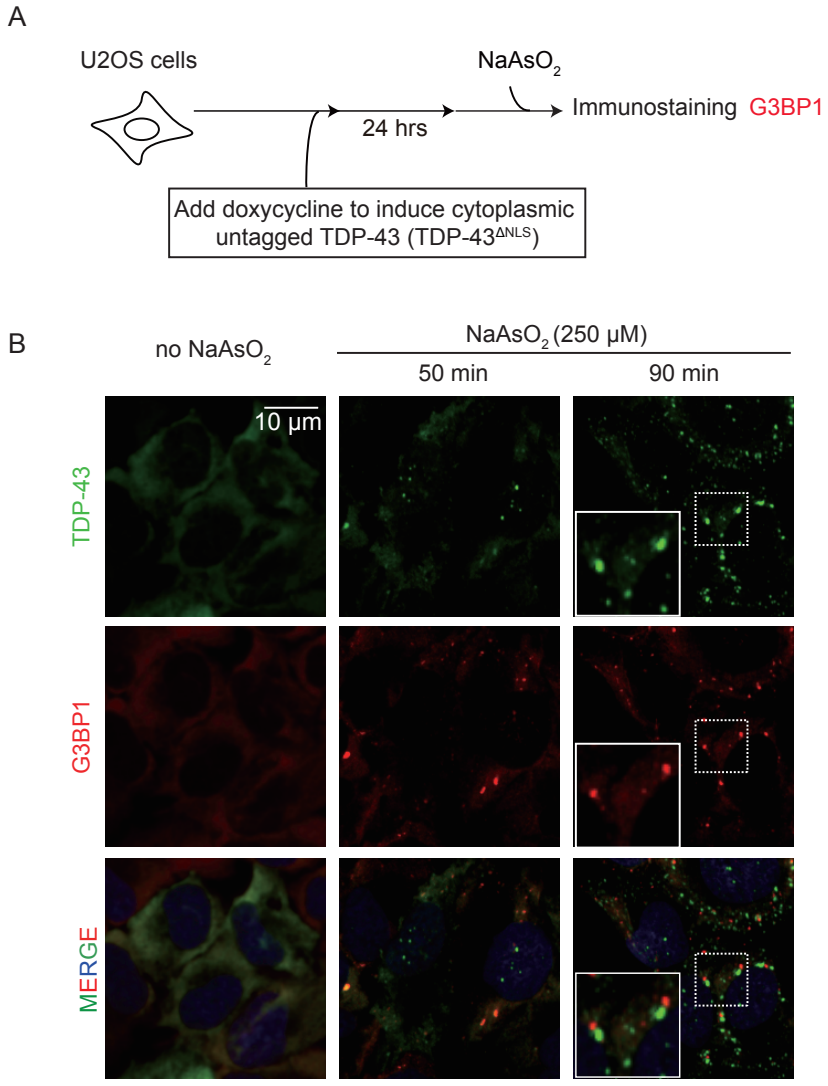

Figure S4: Untagged TDP-43$^{\Delta NLS}$ forms stress granule-independent particles. (Related to Figure 4) (A) Experimental design and (B) immunostaining of untagged cytoplasmic TDP-43 forming stress granule-independent particles after 250 μM sodium arsenite treatment of U2OS cells. G3BP1 was used as a stress granule marker.

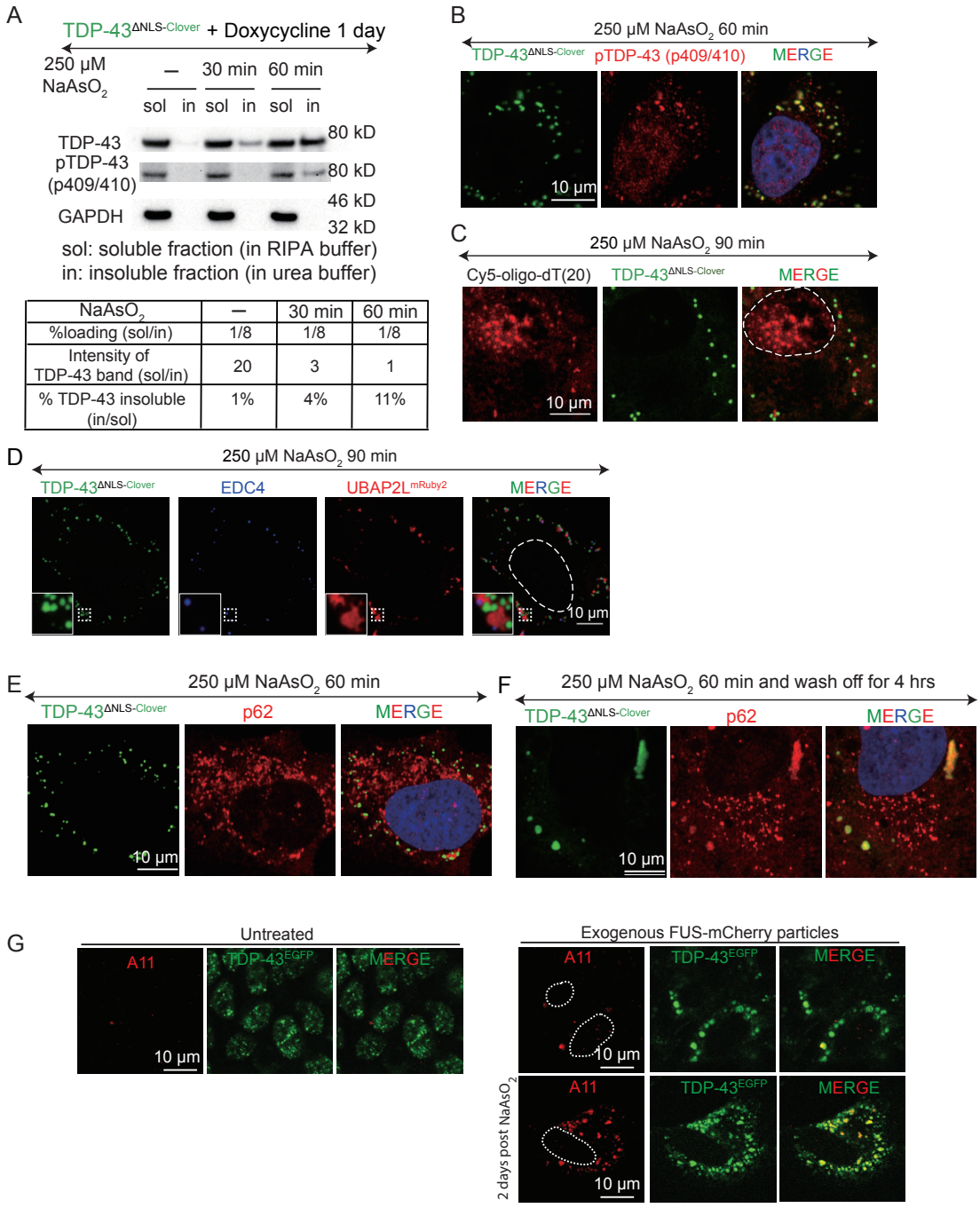

$NaAsO_2$	—	30 min	60 min
%loading (sol/in)	1/8	1/8	1/8
Intensity of TDP-43 band (sol/in)	20	3	1
% TDP-43 insoluble (in/sol)	1%	4%	11%

Figure S5: Stress induces the formation of detergent-insoluble TDP-43 inclusions with the gel-like particles exhibiting amyloid-like features. (Related to Figure 5) (A) Western blot analysis of the proportion of TDP-43 and phospho-TDP-43 in the soluble (RIPA buffer) and insoluble (Urea buffer) fractions without or with 30 min or 60 min of 250 μM sodium arsenite treatment. GAPDH was used as loading control. (B) Representative images of phospho-TDP-43 immunostaining (red) in U2OS cells that accumulate cytoplasmic TDP-$43^{\Delta NLS\text{-}Clover}$ particles (green) after 60 min of 250 μM sodium arsenite treatment. (C) Representative images of mRNA (red) using FISH and cytoplasmic TDP-$43^{\Delta NLS\text{-}Clover}$ particles (green) after 90 min of 250 μM sodium arsenite treatment (red). (D) Representative images of EDC4 (P body) immunostaining (blue) in U2OS cells that form stress granule-independent cytoplasmic TDP-$43^{\Delta NLS\text{-}Clover}$ particles (green) and stress granules indicated by UBAP2L^{mRuby2} (red) after 90 min of 250 μM sodium arsenite treatment. (E-F) Representative images of p62 immunostaining (red) with cytoplasmic TDP-$43^{\Delta NLS\text{-}Clover}$ particles after 60 min of 250 μM sodium arsenite treatment (E) or in the cells with remaining cytoplasmic TDP-$43^{\Delta NLS\text{-}Clover}$ particles after a four hour of wash off of 250 μM sodium arsenite (F). (G) Representative images using confocal microscopy of neuronal-like SH-SY5Y cells inoculated with sonicated FUS^{mCherry} particles in absence or presence of $NaAsO_2$ for 30 minutes (lower panel) and further immunostained with amyloid-oligomers antibody A11 (red) and cytoplasmic TDP-43^{EGFP} (green) after 1 month of fibril treatment or in absence of fibril treatment (left panel).

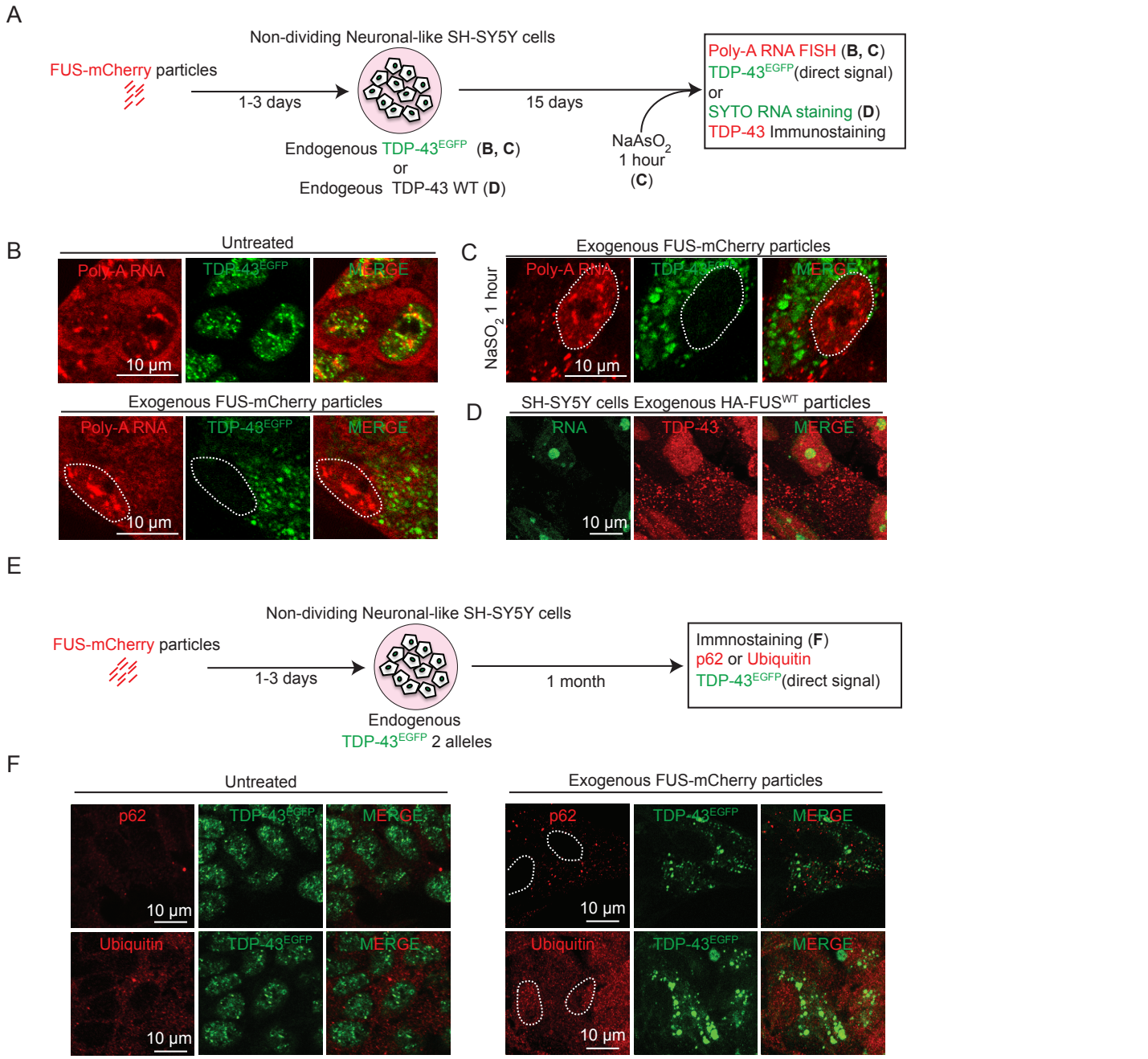

Figure S6: Cytoplasmic TDP-43 de-mixed droplets remain liquid for long periods and do not co-localize with polyA-containing RNAs. (Related to Figure 7) (A) Scheme of the experimental design to assess LLPS properties of endogenous TDP-43^{EGFP} in cells and determine recruitment of RNA within the droplets (B-C) Representative images using confocal microscopy of neuronal-like SH-SY5Y cells (endogenously EGFP tagged TDP-43) 1 month after inoculation of sonicated FUS^{mCherry} particles revealing Poly-A-RNA using fluorescence in situ hybridization (FISH) (grey) and cytoplasmic TDP-43^{EGFP} (green) or (C) subsequently treated for one hour of $NaAsO_2$ (0.5 mM). (D) Neuronal-like SH-SY5Y cells 1 month after inoculation of sonicated FUS^{mCherry} fibrils further stained with SYTO RNA (green) and TDP-43 (red). (E) Scheme of the experimental design to assess LLPS properties of endogenous TDP-43^{EGFP} in cells and determine LLPS features. (F) Representative images using confocal microscopy of neuronal-like SH-SY5Y cells 1 month after inoculation of sonicated FUS^{mCherry} fibrils and further immunostained with p62 (upper panel) or ubiquitin (lower panel) (red) and cytoplasmic TDP-43^{EGFP} (green). Left panel illustrates cells in absence of fibril treatment.

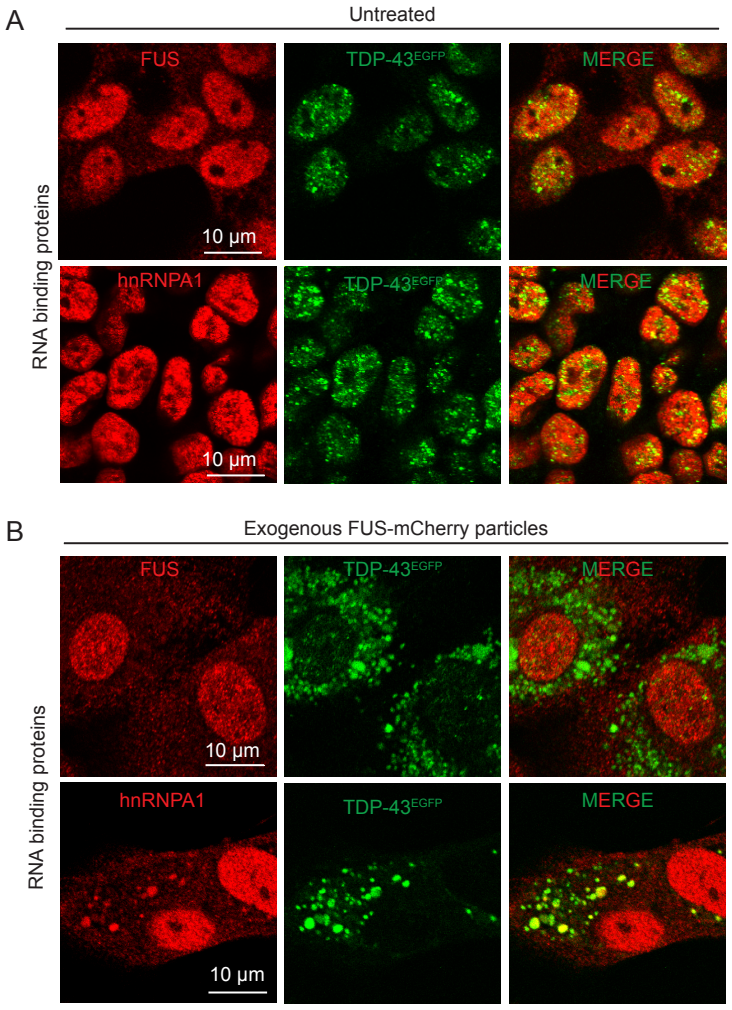

Figure S7: TDP-43 LLPS induces mislocalization of hnRNPA1 and FUS into the cytoplasm due to nuclear import defects. (Related to Figure 8) (A-B) Representative images using confocal microscopy of neuronal-like SH-SY5Y cells in absence of fibril treatment (A) or 1 month after inoculation of sonicated $FUS^{mCherry}$ fibrils (B) and further immunostained with FUS (upper panel), hnRNPA1 (lower panel) (red) and cytoplasmic $TDP\text{-}43^{EGFP}$ (green).